Diptoindonesin G is a middle domain HSP90 modulator for cancer treatment

Received for publication, July 11, 2022, and in revised form, October 31, 2022 Published, Papers in Press, November 14, 2022,
https://doi.org/10.1016/j.jbc.2022.102700

Kristine Donahue[1,‡], Haibo Xie[2,‡], Miyang Li[2], Ang Gao[1], Min Ma[2], Yidan Wang[1], Rose Tipton[3], Nicole Semanik[3], Tina Primeau[3], Shunqiang Li[3], Lingjun Li[2], Weiping Tang[2,*], and Wei Xu[1,*]

From the [1]McArdle Laboratory for Cancer Research, University of Wisconsin-Madison, and [2]School of Pharmacy, University of Wisconsin-Madison, Madison, Wisconsin, USA; [3]Department of Medicine, Division of Oncology, Washington University School of Medicine, St Louis, Missouri, USA

Edited by Philip A. Cole

HSP90 inhibitors can target many oncoproteins simultaneously, but none have made it through clinical trials due to dose-limiting toxicity and induction of heat shock response, leading to clinical resistance. We identified diptoindonesin G (dip G) as an HSP90 modulator that can promote degradation of HSP90 clients by binding to the middle domain of HSP90 (K_d = 0.13 ± 0.02 μM) without inducing heat shock response. This is likely because dip G does not interfere with the HSP90–HSF1 interaction like N-terminal inhibitors, maintaining HSF1 in a transcriptionally silent state. We found that binding of dip G to HSP90 promotes degradation of HSP90 client protein estrogen receptor α (ER), a major oncogenic driver protein in most breast cancers. Mutations in the ER ligand-binding domain (LBD) are an established mechanism of endocrine resistance and decrease the binding affinity of mainstay endocrine therapies targeting ER, reducing their ability to promote ER degradation or transcriptionally silence ER. Because dip G binds to HSP90 and does not bind to the LBD of ER, unlike endocrine therapies, it is insensitive to ER LBD mutations that drive endocrine resistance. Additionally, we determined that dip G promoted degradation of WT and mutant ER with similar efficacy, downregulated ER- and mutant ER-regulated gene expression, and inhibited WT and mutant cell proliferation. Our data suggest that dip G is not only a molecular probe to study HSP90 biology and the HSP90 conformation cycle, but also a new therapeutic avenue for various cancers, particularly endocrine-resistant breast cancer harboring ER LBD mutations.

Estrogen receptor α (ER)-positive tumors are associated with the most favorable prognosis, and ER expression predicts response to endocrine therapies. However, approximately 25% of patients with primary disease, and almost all patients with metastatic disease, will eventually develop resistance to these therapies (1). One established mechanism of resistance in breast cancer patients treated with endocrine therapies is the development of hotspot missense mutations in the ligand-binding domain (LBD) of the gene encoding ER, *ESR1* (2–6). *ESR1* LBD mutations result in a constitutively active receptor and are associated with increased migratory capacity (6) and metastatic potential (7). In addition, mutant ER receptors have reduced ligand-binding affinity to drugs that target the LBD, like fulvestrant, the only FDA-approved selective ER degrader (8–10). Though fulvestrant has been shown to be effective in the metastatic setting, fulvestrant possesses dose-limiting pharmacological properties, such as low bioavailability, and must be administered intramuscularly (11–14). Many new orally bioavailable selective ER degraders are at various stages of clinical evaluation to directly antagonize mutant ER, but none is a pure antiestrogen like fulvestrant, and have mixed agonist and antagonist activity (15–18). Therefore, there is unmet clinical need to develop mechanistically distinct treatment strategies that are insensitive to *ESR1* mutations and do not rely on the ER LBD.

ER stability is affected by multiple factors. Heat shock protein 90 (HSP90) is a molecular chaperone that is responsible for the folding, maturation, activation, and stabilization of over 200 clients. Many of these clients include steroid hormone receptors, such as ER (19, 20). HSP90 maintains ER in a ligand-binding conformation and protects ER from proteasomal degradation (21). HSP90 is composed of three domains. The N-terminal domain is responsible for ATP hydrolysis and contains a druggable ATP-binding pocket. The middle (M) domain is responsible for assembling unfolded client proteins and can bind some cochaperones. The C-terminal domain is primarily involved in homodimerization of HSP90 and contains a highly conserved MEEVD peptide where cochaperones bind. HSP90 in cancer behaves very differently from HSP90 in normal cells and protects overexpressed and mutated oncoproteins, mediating oncoprotein addiction (19). Interestingly, HSP90 inhibitors generally have a higher affinity for HSP90 in tumors than in normal cells and accumulate selectively in tumors because soluble HSP90 in tumor cells is assembled in multichaperone complexes that are more active than HSP90 in normal cells, which is in a noncomplexed, inactive form (22), making HSP90 an attractive and highly sought-after cancer target.

HSP90 collaborates with the ubiquitin proteasome system, another primary regulator of ER stability, that is critical for

‡ These authors contributed equally to this work.
* For correspondence: Wei Xu, wxu@oncology.wisc.edu; Weiping Tang, weiping.tang@wisc.edu.

maintaining protein homeostasis and unfolded protein turnover (23, 24). Ubiquitin ligases (E3) catalyze the covalent binding of ubiquitin to lysine residues of target proteins (23, 24) for degradation by the 26S proteasome. There are estimated to be over 600 E3 ligases (25). Some of the most well-known E3 ligases that regulate ER stability include MDM2 (26), CHIP (27), BARD1 (28), BRCA1 (29), SKP2 (30), and E6AP (31).

HSP90 can be pharmacologically inhibited using HSP90 inhibitors that belong to the benzoquinone antibiotic family. Geldanamycin, as well as its analogs tanespimycin and alvespimycin, binds to the N-terminal ATP-binding pocket, inhibiting HSP90's ATPase activity, which is essential for its chaperone functions (32, 33). ATP binding and hydrolysis are coupled to the "opening" and "closing" of HSP90 protomers (20, 34, 35) and these structural rearrangements regulate the interactions with cochaperones and client proteins (36). Inhibition of HSP90 results in inhibition of the chaperoning cycle (20, 34, 35), recruitment of E3 ligases, and the degradation of client proteins by the 26S proteasome (27, 37).

Unfortunately, though amino-terminal–targeting HSP90 inhibitors have been tested in over 100 clinical trials as a single agent and in combination with other drugs in many cancer types, the toxicity, particularly to hepatocytes in the context of benzoquinone ansamycin derivatives (38), and lack of clinical response observed have precluded FDA approval of HSP90 inhibitors. Inhibitors that target the N-terminus induce heat shock response (HSR), which is one major mechanism of resistance to HSP90 inhibition. This is caused by derepression of HSF1, which subsequently upregulates HSPs (39–41). HSPs regulated by HSF1, such as HSP27, HSP40, HSP70, and HSP90, protect cells from apoptosis and inhibit cytochrome C, as well as TNF-mediated cell death (42). As a result, there is strong rationale to develop better tolerated and mechanistically distinct HSP90 inhibitors. A handful of middle and C-terminal inhibitors have been developed and can circumvent HSR but have never been tested in clinical trials.

Diptoindonesin G (dip G) was originally reported by our group to be a modulator of the E3 ligase CHIP and has been studied in the context of ER+ breast cancer (43, 44), as well as in AML (45), triple negative breast cancer (46), and prostate cancer (47). The anticancer effects of dip G have also been observed *in vivo* in both triple negative breast cancer cell line MDA-MB-231–derived xenograft models (46), as well as castration-resistant prostate cancer 22Rv1-derived xenograft models (47). Mao *et al* demonstrated that dip G could induce AR degradation in a CHIP-dependent manner in human prostate cancer cells and manipulating CHIP expression affected dip G sensitivity (47). In addition, they showed that dip G enhanced the efficacy of tanespimycin, an HSP90 inhibitor, and enzalutamide, an AR antagonist, in prostate cancer cell lines and *in vivo* prostate cancer models (47). Zhao *et al* showed that dip G could promote degradation of ER α but also reciprocally stabilize ER β, implicating a commonly shared E3 ligase, CHIP (43). When CHIP was knocked down using shRNA, dip G–mediated ER α degradation and ER β stabilization was abrogated, indicating that CHIP is essential for dip G's mechanism of action (43). In addition, Zhao *et al* also showed that dip G increased proximity of CHIP and ER α. However, it remains unclear whether dip G directly targets CHIP, ER, modulates another component of the HSP90–ER–CHIP ternary complex, or acts as a molecular glue.

This study focuses on elucidating the mechanism of action of dip G and its potential clinical applications. Herein, we show that dip G does not regulate CHIP activity but rather, is an HSP90 modulator which, unlike previously described amino and carboxy-terminal targeting inhibitors, targets the middle domain of HSP90. To our knowledge, only a handful of other compounds, all of which are natural products, are known to bind to the middle domain. Unlike tanespimycin, dip G does not upregulate HSPs to the same extent and only affects a subset of the proteins affected by tanespimycin, which indicates that it may be more tolerable to normal cells. We found that dip G promoted the degradation of both WT and mutant ER at similar efficacies. This resulted in subsequent inhibition of both ER-regulated gene expression and proliferation of breast cancer cell lines expressing mutant ER. In addition, we observed ER degradation, downregulation of ER target genes, as well as growth inhibition in ER-positive breast cancer patient–derived xenograft organoids (PDXOs) treated with dip G. Therefore, dip G represents a novel therapeutic avenue to treat endocrine-resistant breast cancer caused by LBD mutations.

Results

Dip G and its analog deoxy-dip G promote ER degradation

We first compared dip G's ability to promote ER α degradation to that of either known ER ligands or HSP90 inhibitors by treating MCF7 cells with 10 nM 17-β estradiol (E2), 1 μM 4-hydroxytamoxifen (OHT), 100 nM fulvestrant, 1 μM tanespimycin, as well as 10 μM dip G. As expected, E2 induced significant degradation of ER. OHT treatment stabilized ER and resulted in the accumulation of ER levels that were even higher than that of dimethyl sulfoxide (DMSO) treatment. Fulvestrant, tanespimycin, and dip G resulted in similar levels of degradation to that of E2 (Fig. 1*A*). These results were validated for dip G by Western blot (Fig. 1*B*). In addition, a modified dip G analog, deoxy-dip G, which lacks a hydroxyl group and has been shown to have increased efficacy to degrade ER α and stabilize ER β[44], results in similar dose-dependent degradation of ER (Fig. 1*C*). To quantitatively measure the ability of dip G to induce ER degradation, following hormone starvation, we treated MCF7 cells with increasing concentrations of fulvestrant (1–1000 nM), dip G (0.1–10 μM), or tanespimycin (0.5–4 μM) for 24 h. ER levels were evaluated using an ER ELISA. Fulvestrant, dip G, and tanespimycin induced dose-dependent degradation of ER. Treatment with 1 μM fulvestrant, the highest nonphysiologically relevant dose used in this experiment, 10 μM dip G, and 4 μM tanespimycin resulted in a 64.8%, 72.8%, and 58.3% (Fig. 1*D*) reduction in ER, respectively, as compared to vehicle treatment (44).To quantitatively measure the ability of dip G to decrease ER

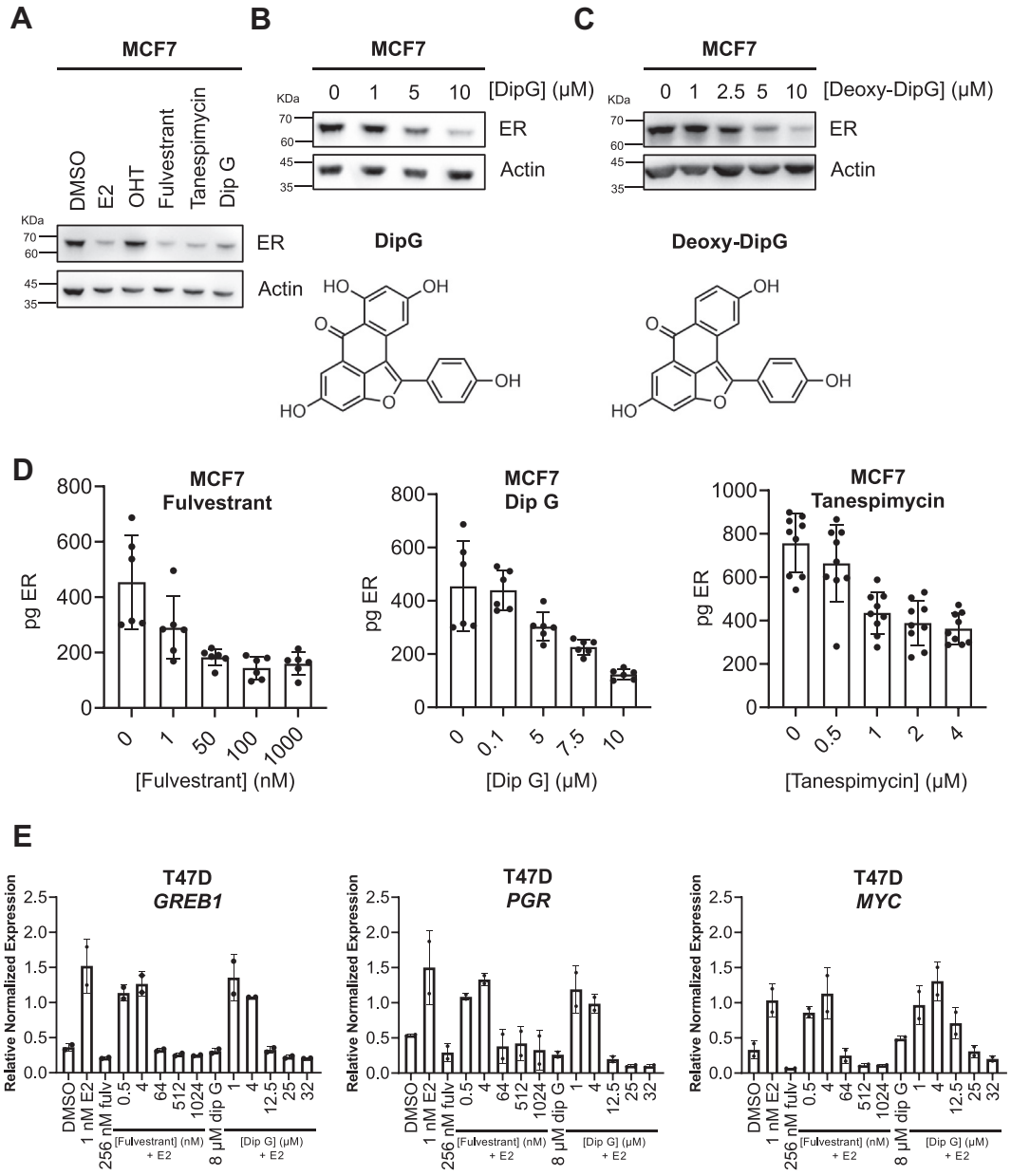

Figure 1. Dip G promotes ER degradation in MCF7 cells. *A*, Western blot of ER levels in MCF7 cells treated with DMSO, 10 nM 17β-estradiol (E2), 1 μM 4-hydroxytamoxifen (OHT), 100 nM fulvestrant, 1 μM tanespimycin, or 10 μM dip G for 6 h. MCF7 cells were hormone starved for 3 days prior to treatment. Actin was used as a loading control. Three independent experiments with three biological replicates. One representative blot is shown. *B*, (Upper) Western blot of ER levels in MCF7 cells treated with DMSO, 1, 5, or 10 μM dip G for 24 h. MCF7 cells were hormone starved for 3 days prior to treatment. Actin was used as a loading control. Three independent experiments with three biological replicates. One representative blot is shown. (Lower) Molecular structure of diptoindonesin G. *C*, (Upper) Western blot of ER levels in MCF7 cells treated with DMSO, 1, 2.5, 5, or 10 μM deoxy-dip G for 24 h. MCF7 cells were hormone starved for 3 days prior to treatment. Actin was used as a loading control. Three independent experiments with three biological replicates. One representative blot is shown. (Lower) Molecular structure of deoxy-diptoindonesin G. *D*, ELISA assay of ER levels in MCF7 cells following treatment with DMSO, 1, 10, 50, and 1000 nM of fulvestrant, DMSO, 0.1, 5, 7.5, and 10 μM dip G, or DMSO, 0.25, 0.5, 1, 2, and 4 μM tanespimycin for 24 h. MCF7 cells were hormone starved for 3 days prior to treatment. ER protein levels were normalized to 1×10^7 cells for fulvestrant and dip G and to total protein concentration for tanespimycin. Two independent experiments with three biological replicates and two technical replicates were carried out for fulvestrant and dip G. Three independent experiments with three biological replicates and two technical replicates were carried out for tanespimycin. Individual biological replicates are plotted. Data are represented as mean ± SD. *E*, RT-qPCR analysis of ER target gene *GREB1*, *PGR*, *and MYC* expression in T47D cells treated with DMSO, 1 nM E2, or 1 nM E2 plus increasing concentrations of fulvestrant (0.5–1024 nM) or dip G (1–32 μM) for 24 h. Cells were hormone starved for 3 days prior to treatment. Expression was normalized to *18s rRNA*. Two independent experiments with two biological replicates and three technical replicates were carried out. Individual biological replicates are plotted. Data are represented as mean ± SD. dip G, diptoindonesin G; ER, estrogen receptor.

transcriptional activity, following hormone starvation, we treated T47D cells with increasing concentrations of fulvestrant (0.5–1024 nM) or dip G (1–32 μM) for 24 h. Expression of ER target genes *GREB1*, *PGR*, and *MYC* were measured using RT-qPCR (Fig. 1*E*). Both compounds resulted in dose-dependent downregulation of all three genes.

Dip G mediates ER degradation through the 26S proteasome independently of CHIP

To test whether dip G promotes ER degradation through the 26S proteasome, MCF7 cells that were hormone starved for 3 days were treated with 10 μM dip G, 0.5 μM bortezomib, a proteasome inhibitor, or a combination of dip G and bortezomib for 24 h. Dip G promoted ER degradation alone. Treatment with bortezomib slightly decreased ER levels but also resulted in the accumulation of ubiquitinated proteins. Bortezomib treatment abrogated dip G–mediated ER degradation, indicating that dip G promotes ER degradation through the 26S proteasome (Fig. 2*A*, Fig. S1A).

Previously, our group showed that CHIP was required for dip G–induced ER degradation using ER-negative cell line Hs578T overexpressing flag-tagged ER. When CHIP was knocked down with shRNA, ER degradation was abrogated (43). To test what proteins are affected by dip G treatment in the presence and absence of CHIP, we performed mass spectrometry analysis of LCC2 shControl and LCC2 shCHIP cells treated with 10 μM dip G. LCC2 is a tamoxifen-resistant clone of MCF7 (48). We found that 245 proteins were downregulated and 233 proteins were upregulated in the shControl cells, and 297 proteins were downregulated and 334 proteins were upregulated in the shCHIP cells in response to dip G treatment. To our surprise, we saw significant downregulation of ER protein in both cell lines (Fig. 2, *B* and *C*, Table S1). 27.3% of the downregulated proteins overlapped in the two groups, and 35.8% of the downregulated proteins were shared. Fifty five percent of the total changed proteins in the shControl group were shared with the changed proteins in the shCHIP group, indicating that more than half of the total significantly changed proteins are regulated by dip G in a CHIP-independent manner (Fig. S1B). We validated this effect in MCF7 shControl and MCF7 shCHIP cells (43) by Western blot. In agreement with the mass spectrometry results, a 24-h treatment with 10 μM dip G after hormone starvation induced significant ER downregulation in the presence and absence of CHIP (Fig. 2*D*). In addition, basal ER levels appeared to be higher in the MCF7 shCHIP cells, indicating that CHIP does indeed regulate ER stability in these cells (Fig. 2*D*, Fig. S1C). To eliminate the possibility that residual levels of CHIP were mediating dip G's effects, we designed gRNAs targeting the second exon of *STUB1,* encoding CHIP, and generated two CHIP KO cell lines in MCF7 using CRISPR/cas9 (49). Absence of full-length CHIP protein was confirmed using Western blot, as well as mass spectrometry (Fig. 2*E*, Table S2). To test whether dip G could promote degradation of ER in a CHIP-dependent manner in CHIP KO cell lines, parental MCF7 as well as both MCF7 CHIP KO clones were treated with 10 μM dip G for 24 h. In parental MCF7, ER was degraded in response to dip G. In both MCF7 CHIP KO clones, ER was also degraded in response to dip G treatment (Fig. 2, *F* and *G*). This effect was also observed using deoxy-dip G (Fig. S1, *D* and *E*).

To better understand the discrepancy between the results from Hs578T-ER-LUC, MCF7, and LCC2, we measured the expression of E3 ligases that regulate ER stability, including MDM2, CHIP, and E6AP in 13 different ER +, HER2+, and triple negative breast cancer cell lines by Western blot. Expression levels of these proteins varied across cell lines, even within the same molecular subtype. MCF7 had higher expression of all E3 ligases known to regulate ER than HS578T (Fig. S2A).

Dip G analog deoxy-dip G binds to the middle domain of HSP90

We used dip G analog deoxy-dip G as well as compounds known to interact with different domains of HSP90 in fluorescence polarization assays to further probe dip G's direct target and measure the interaction of deoxy-dip G with CHIP, ER, and HSP90. Deoxy-dip G has a fluorescence emission between 485 to 520 nm and can be a used as a fluorescent tracer (Fig. S3A). The N-terminus of HSP90 is specific to adenosine nucleotides with an intact adenine ring, such as ATP, as well as compounds that are structurally similar to ATP, like geldanamycin or its analog tanespimycin. The C-terminus can bind to Novobiocin and (-)-epigallocatechin gallate (EGCG) (50). The C-terminus of HSP90 is more promiscuous with the kind of nucleotides it can interact with and binds both ATP as well as GTP (51). The K_d of deoxy-dip G to HSP90 was 310 nM (Fig. 3*A*), while the K_d of deoxy-dip G to CHIP and ER was 9.6 μM (Fig. 3*B*) and 3.1 μM (Fig. 3*C*), respectively, indicating that HSP90 is more likely to be deoxy-dip G's direct target. The MEEVD peptide is found at the C-terminus of HSP90 and binds to cochaperones with a tetratricopeptide repeat domain, like CHIP. The literature value of 17-β estradiol binding to ER is 0.21 nM[8], and as a positive control, we were able to compete Fluormone ES2 off with 17β-estradiol (Fig. S3B). By comparison, we found the K_d of geldanamycin-FITC was 509 nM, which is similar to literature values (Fig. S3C) (52). In addition, we measured the K_d of CHIP to an 5FAM-MEEVD peptide, which was 1.60 μM (Fig. S3D). This indicates that deoxy-dip G binds to HSP90 with a similar affinity as geldanamycin. However, deoxy-dip G could neither be competed off by geldanamycin (Fig. S3E) nor radicicol (Fig. S3G), implying that deoxy-dip G does not bind to HSP90's N-terminus, but deoxy-dip G could be competed off by ATP (Fig. S3F). Deoxy-dip G also could neither be competed off by GTP (Fig. S3H), novobiocin (Fig. S3I), nor EGCG (Fig. S3J), indicating that it is unlikely that deoxy-dip G binds to the C-terminus.

Next, we determined the domain of HSP90 to which deoxy-dip G binds by expressing and purifying GST-tagged HSP90 protein fragments from plasmids corresponding to the N-terminus (AA 9–236), M-domain (AA 272–617), and C-terminus (AA 626–732) (53). The GST tag was cleaved using thrombin, and these fragments were used for fluorescence polarization assays (Fig. 3*G*). We found that deoxy-dip G's K_d to the middle domain was 130 nM (Fig. 3*D*), equivalent to the K_d of deoxy-dip G to full-length HSP90 (310 nM). In contrast, we found that deoxy-dip G bound to the N fragment of 13.77 μM (Fig. 3*E*) and to the C fragment with a K_d of 8.01 μM (Fig. 3*F*). However, even known C-terminal inhibitors, such as cisplatin and novobiocin, are not known to bind with high affinity to the C-terminal

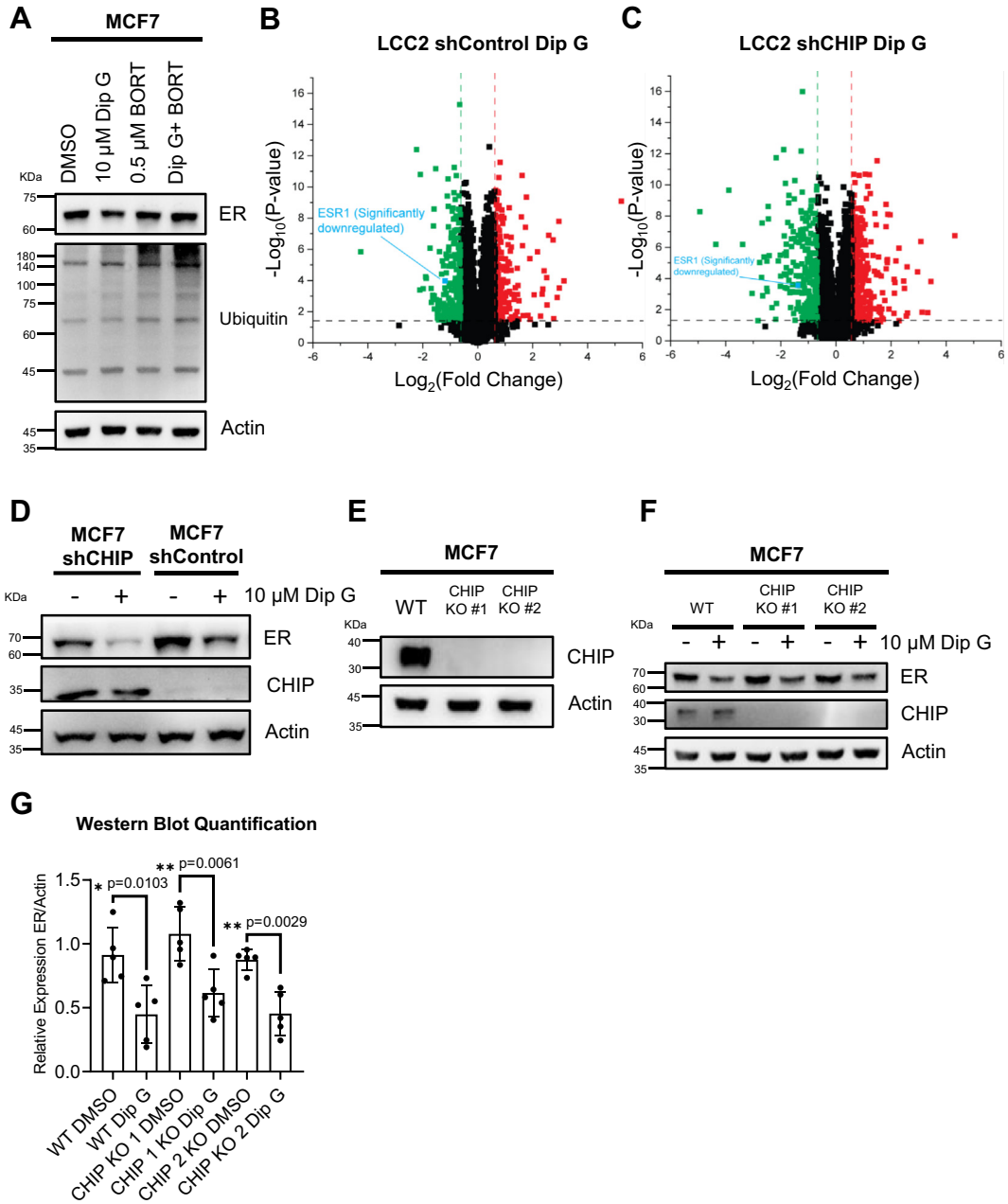

Figure 2. CHIP is not required for dip G-mediated ER degradation through the 26S proteasome. *A*, Western blot of ER and ubiquitin levels in MCF7 cells treated with DMSO, 10 μM dip G, 0.5 μM bortezomib (BORT), or a combination of the two compounds, for 6 h. MCF7 cells were hormone starved for 3 days prior to treatment. Actin was used as a loading control. Three independent experiments with three biological replicates were carried out. One representative blot is shown. *B*, volcano plot of proteins significantly downregulated (*green*) and upregulated (*red*) in MCF7 LCC2 shControl cells in response to 10 μM dip G treatment. Log_2 (fold change) is plotted on the x-axis and significance, or the $-log_{10}$(*p*-value) is plotted on the y-axis. Proteins not significantly changed are indicated in *black*. ESR1 (ER), highlighted in *cyan*, was significantly decreased by dip G treatment in both cell lines. One independent experiment with three biological replicates and three technical replicates was carried out. *C*, volcano plot of proteins significantly downregulated (*green*) and upregulated (*red*) in MCF7 LCC2 shCHIP cells in response to 10 μM dip G treatment for 24 h. Log_2 (fold change) is plotted on the x-axis and significance, or the $-log_{10}$(*p*-value) is plotted on the y-axis. Proteins not significantly changed are indicated in *black*. ESR1 (ER), highlighted in *cyan*, was significantly decreased by dip G treatment in both cell lines. One independent experiment with three biological replicates and three technical replicates was carried out. *D*, Western blot of ER and CHIP levels in MCF7 shControl and MCF7 shCHIP cells treated with DMSO or 10 μM dip G for 24 h. MCF7 cells were hormone starved for 3 days prior to treatment. Actin was used as a loading control. Three independent experiments with three biological replicates were carried out. One representative blot is shown. *E*, Western blot of CHIP levels in MCF7 CHIP KO clones #1 and #2 cells. Actin was used as a loading control. Three independent experiments with three biological replicates were carried out. One representative blot is shown. *F*, Western blot of ER and CHIP levels in MCF7 parental and CHIP KO clone #1 and #2 cells treated with DMSO or 10 μM dip G for 24 h. Cells were hormone starved for 3 days prior to treatment. Actin was used as a loading control. Three independent experiments with three biological replicates were carried out. One representative blot is shown. *G*, quantification of the Western blot shown in (F) individual biological replicates are plotted. Data are represented as the mean ± SD. Significance was determined using an unpaired Welch's *t* test. dip G, diptoindonesin G; ER, estrogen receptor.

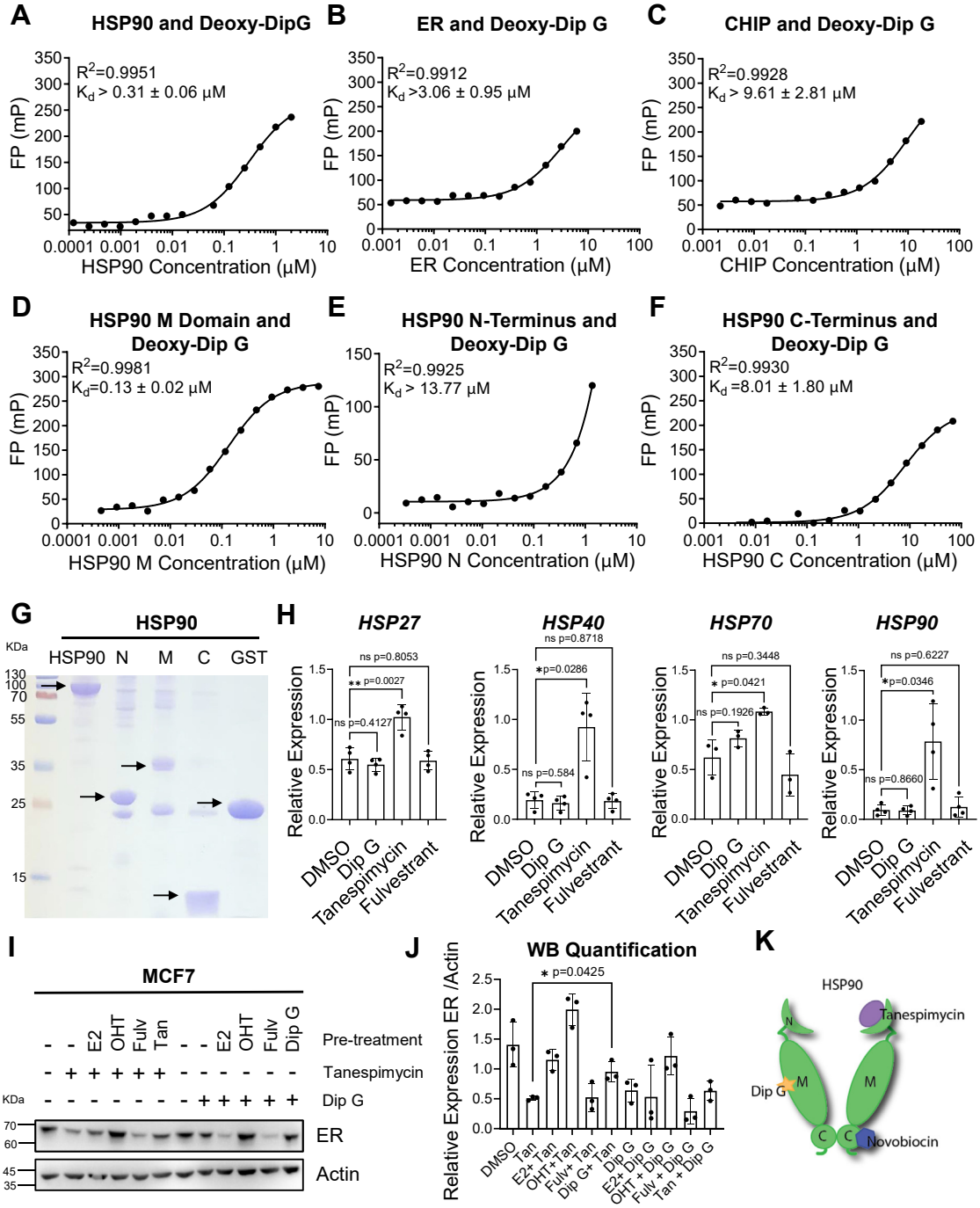

Figure 3. Dip G is a middle domain HSP90 modulator. *A*, fluorescence polarization plots measuring the K_d (bottom right corner of each plot) of deoxy-dip G to ER. Fluorescence polarization (in units of mP) is plotted on the y-axis (linear scale) and the protein concentration is plotted on the x-axis (logarithmic scale). The concentration of deoxy-dip G used was 1 μM. *B*, fluorescence polarization plots measuring the K_d (bottom right corner of each plot) of deoxy-dip G to HSP90. Fluorescence polarization (in units of mP) is plotted on the y-axis (linear scale) and the protein concentration is plotted on the x-axis (logarithmic scale). The concentration of deoxy-dip G used was 1 μM. *C*, fluorescence polarization plots measuring the K_d (bottom right corner of each plot) of deoxy-dip G to CHIP. Fluorescence polarization (in units of mP) is plotted on the y-axis (linear scale) and the protein concentration is plotted on the x-axis (logarithmic scale). The concentration of deoxy-dip G used was 1 μM. *D*, fluorescence polarization plots measuring the K_d (bottom right corner of each plot) of deoxy-dip G to the HSP90 M domain. Fluorescence polarization (in units of mP) is plotted on the y-axis (linear scale) and the protein concentration is plotted on the x-axis (logarithmic scale). The concentration of deoxy-dip G used was 1 μM. *E*, fluorescence polarization plots measuring the K_d (bottom right corner of each plot) of deoxy-dip G to the HSP90 N-terminus. Fluorescence polarization (in units of mP) is plotted on the y-axis (linear scale) and the protein concentration is plotted on the x-axis (logarithmic scale). The concentration of deoxy-dip G used was 1 μM. *F*, fluorescence polarization plots measuring the K_d (bottom right corner of each plot) of deoxy-dip G to the HSP90 C-terminus. Fluorescence polarization (in units of mP) is plotted on the y-axis (linear scale) and the protein concentration is plotted on the x-axis (logarithmic scale). The concentration of deoxy-dip G used was 1 μM. *G*, Coomassie-stained SDS-PAGE gel of full length HSP90 (FL-HSP90), purified HSP90 N-domain (N), HSP90 middle domain (M), and HSP90 C domain (C). The expected molecular weights are as follows: FL-HSP90 - 90 KDa, GST-HSP90 N (AA 9–236) - 55 KDa, HSP90 N - 26 KDa, GST-HSP90 M (AA 272–617) -62 KDa, HSP90 M - 41 KDa, GST-HSP90 C (AA 626–732) -38 KDa, HSP90 C -11.91 KDa, GST - 26 KDa. *H*, RT-qPCR analysis of *HSP27, HSP40*, *HSP70*, and *HSP90* expression in MCF7 cells treated with DMSO, 10 μM dip G, 2 μM tanespimycin, or 40 μM novobiocin in full medium for 3 hours. Expression was normalized to *18s rRNA*. Four independent experiments with four biological replicates and three technical replicates were carried out. For *HSP70*, only three independent experiments with three

domain of HSP90 (50). Our results indicate that dip G likely binds to the middle domain of HSP90, as compared to tanespimycin, which binds to the N-terminus, and novobiocin, which binds to the C-terminus (Fig. 3*K*).

Tanespimycin and dip G have distinct mechanisms for targeting HSP90

Many N-terminal HSP90 inhibitors can derepress HSF1, leading to induction of HSR, a major mechanism of resistance to HSP90 inhibitors. We evaluated dip G's ability to induce HSR by incubating MCF7 cells with dip G, tanespimycin, or novobiocin for 3 h and measuring the expression of *HSP27*, *HSP40*, *HSP70*, *and HSP90* by RT-qPCR, all of which are upregulated in response to heat shock and protect cells from proteotoxic stress (54). Tanespimycin, an N-terminal inhibitor, was the only compound to upregulate all HSPs (Fig. 3*H*). Novobiocin, a C-terminal HSP90 inhibitor that is not known to induce HSR, and dip G had no effect on HSP levels (50, 55) (Fig. 3*H*).

Fan *et al.* established that CHIP is required for geldanamycin-induced ER degradation. ER ligands, such as E2, OHT, can promote ER–HSP90 complex disassembly, which completely abolishes geldanamycin-induced ER degradation (27). We wondered if ligand binding would disrupt dip G–induced ER degradation, as has been previously reported for geldanamycin.

To test this, MCF7 cells were pretreated with vehicle, tanespimycin (tan), or dip G for 30 min, followed by a five-and-a-half-hour treatment with ER ligands, including E2, 4-OHT, or fulvestrant. Though E2 is an ER agonist, transcriptional activation of ER is coupled with ER degradation. This degradation mechanism is distinct from that of tanespimycin and dip G, where degradation is coupled to target gene downregulation. Our results showed that dip G and tanespimycin alone promoted ER degradation (Fig. 3, *I* and *J*). Cotreatment of either dip G or tanespimycin with OHT stabilized ER and abolished both tanespimycin's and dip G's ability to promote ER degradation (Fig. 3, *I* and *J*). The effect of fulvestrant with either tanespimycin or dip G was additive and induced ER degradation (Fig. 3, *I* and *J*). However, cotreatment with E2 and tanespimycin stabilized ER compared to tanespimycin alone (Fig. 3, *I* and *J*). This is likely because ER is already bound to E2 and is no longer complexed with HSP90. With E2 and dip G cotreatment, the combination was additive. In addition, tanespimycin and dip G cotreatment abrogated each compound's effects on ER degradation, indicating that they have the same target and that HSP90 is required for dip G's function (Fig. 3, *I* and *J*). This was also observed using deoxy-dip G (Fig. S3, *K* and *L*).

Towards further distinguishing tanespimycin and dip G, we measured their effects on the proteome. MCF7 cells were treated with concentrations of tanespimycin and dip G that resulted in comparable ER downregulation (Fig. 4*A*). Using label-free MS, over 450 proteins were affected by tanespimycin, but less than 200 proteins were affected by dip G treatment (Fig. 4, *B* and *C*). Specifically, 92 proteins were downregulated and 79 proteins were upregulated by dip G (Fig. 4*B*), respectively, and 225 proteins were downregulated and 239 proteins were upregulated by tanespimycin (Fig. 4*C*). When comparing the proteins downregulated by tanespimycin and dip G, 29% of the dip G downregulated proteins fall within the tanespimycin downregulated proteins, and 48% of the dip G upregulated proteins fall within the tanespimycin upregulated proteins (Fig. 4, *D* and *E*). Proteins affected by tanespimycin include known HSP90 clients and cochaperones, such as ERBB2, DDR1, and BAG1 (Table S3). Dip G regulates a subset of tanespimycin-affected proteins but also regulates a unique set of proteins.

We used PRISM, a pan-cancer pooled screening developed by Broad Institute, to profile deoxy-dip G's effect on cell viability across 770 cancer cell lines, with the goal of identifying small molecules with a similar cytotoxicity profile previously determined using this platform, further informing about the mechanism of action of dip G and its analogs (56, 57). Each cell line has a stably integrated DNA barcode and is treated with compounds for 5 days. Bar codes are recovered and used to interpolate viability and relative cell line sensitivity. We found that many different tissue lineages were sensitive to deoxy-dip G, including bone, leukemia, lymphoma, rhabdoid, and rhabdomyosarcoma lineages (Fig. S4). Though PRISM is an effective assay for quickly screening hundreds of cells lines at once to test for sensitivity to a compound of interest, it has difficulty predicting allosteric inhibitors, as well as sensitivity to very specific mutations.

Dip G inhibits the ER Y537S mutant in ER+ breast cancer cells

Though many cancer models are sensitive to dip G, we hypothesized that dip G could be an effective therapy in the context of endocrine-resistant breast cancer, where mutations in the LBD of ER reduce the efficacy of ER antagonists. Because dip G promotes ER degradation through HSP90 in a ligand-independent manner, we examined dip G's impact on ER Y537S degradation, transcriptional activity, and cell growth in MCF7 to test this hypothesis.

To quantitatively measure the ability of dip G to induce ER Y537S degradation, we treated MCF7 cells with a single allele knock-in of ER Y537S (58) with increasing concentrations of

biological replicates and three technical replicates were run. Significance was determined using an unpaired *t* test with Welch's correction. Individual biological replicates are plotted. Data are represented as mean ± SD. *I*, Western blot of ER levels in MCF7 cells pretreated with 10 μM dip G or 1 μM tanespimycin for 0.5 h and then treated with DMSO, 10 nM 17β-estradiol (E2), 1 μM 4-hydroxytamoxifen (OHT), 100 nM fulvestrant (Fulv), 1 μM tanespimycin (Tan), or 10 μM dip G for 5.5 h. MCF7 cells were hormone starved for 3 days prior to treatment. Actin was used as a loading control. Three independent experiments with three biological replicates were carried out. One representative blot is shown. *J*, quantification of the Western blot shown in (*I*) individual biological replicates are plotted. Data are represented as the mean ± SD. Significance was determined using an unpaired Welch's *t* test. *K*, model of HSP90 showing that tanespimycin binds to the N-terminus, dip G binds to the middle domain, and novobiocin binds to the C-terminus. dip G, diptoindonesin G; ER, estrogen receptor; HSP90, Heat shock protein 90.

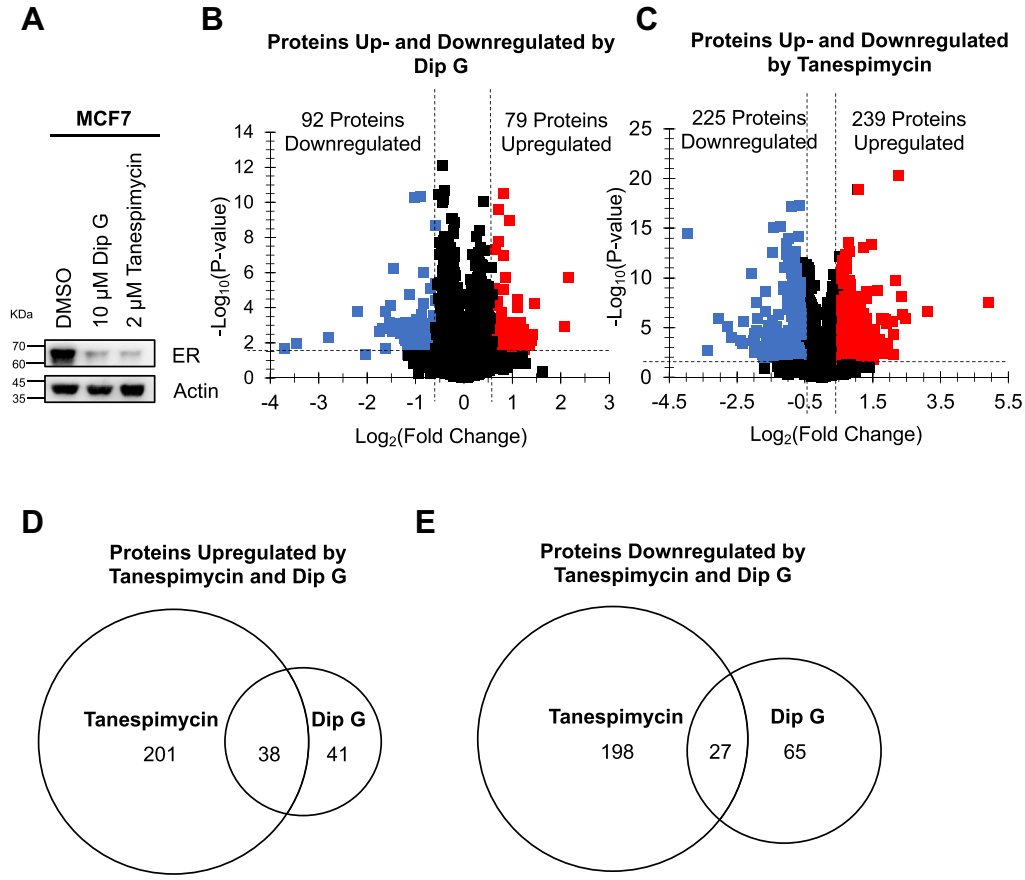

Figure 4. Dip G regulates a subset of tanespimycin-affected proteins. *A*, Western blot of ER in MCF7 cells treated with 10 μM dip G or 2 μM tanespimycin for 24 h. Actin was used as a loading control. Three independent experiments with three biological replicates were carried out. One representative blot is shown. *B*, volcano plot of proteins significantly downregulated (*blue*) and upregulated (*red*) in MCF7 cells treated with 10 μM dip G. Log_2 (fold change) is plotted on the x-axis and significance, and the $-log_{10}$(*p*-value) is plotted on the y-axis. Proteins not significantly changed are indicated in *black*. Three biological replicates with three technical replicates were carried out. *C*, volcano plot of proteins significantly downregulated (*blue*) and upregulated (*red*) in MCF7 cells treated with 2 μM tanespimycin (*right*). Log_2 (fold change) is plotted on the x-axis and significance, and the $-log_{10}$(*p*-value) is plotted on the y-axis. Proteins not significantly changed are indicated in *black*. Three biological replicates with three technical replicates were carried out. *D*, Venn diagrams comparing proteins significantly upregulated by both dip G and tanespimycin. Proteins unique to tanespimycin are on the *left*, and proteins unique to dip G are on the *right*. Proteins shared by both are shown in the overlapping region. *E*, Venn diagrams comparing proteins significantly downregulated by both dip G and tanespimycin. Proteins unique to tanespimycin are on the *left*, and proteins unique to dip G are on the *right*. Proteins shared by both are shown in the overlapping region. dip G, diptoindonesin G; ER, estrogen receptor.

dip G, fulvestrant, or tanespimycin for 24 h. Heterozygous expression of both WT and Y537S ER recapitulates what is often observed in patients. ER levels were evaluated using an ER ELISA. Unlike in the WT ER context, where fulvestrant, dip G, and tanespimycin induced dose-dependent degradation of ER (Fig. 1*D*), ER Y537S protein was resistant to fulvestrant treatment, as observed by a plateau response (Fig. 5*A*). Dip G and tanespimycin induced a dose-dependent decrease in ER Y537S protein (Fig. 5*A*), as previously observed in MCF7 WT (Fig. 1*D*). Treatment with 1 μM fulvestrant, 10 μM dip G, and 4 μM tanespimycin resulted in a 51.5%, 71.5%, and 68.4% reduction in ER, respectively, as compared to vehicle treatment. This is in contrast to the 64.8%, 72.8%, and 58.3% reduction, respectively, seen in WT ER-expressing MCF7 (Fig. 1*D*), indicating that only the effects of fulvestrant are affected by mutant ER. However, in this experiment, we cannot distinguish between WT ER and ER Y537S, as we do not have a mutant ER-specific antibody, and mutant ER-expression is heterozygous in this cell line.

Because we observed ER Y537S protein levels were decreased by dip G, we wanted to know whether a decrease in protein levels correlated to downregulation of ER Y537S protein's transcriptional activity. We performed RNA-seq on T47D WT and T47D Y537S cells (5) treated with either DMSO or 10 μM dip G for 24 h, followed by differential gene expression analysis and Gene Set Enrichment Analysis (GSEA). Hallmark gene sets "estrogen response early" and "estrogen response late" were significantly downregulated by dip G treatment (Fig. 5, *B* and *C*). Canonical ER target genes such as GREB1, PGR, and MYC were also significantly downregulated (Table S3). Epithelial mesenchymal transition, which is consistent with the mutant's reported metastatic phenotype, was also downregulated. Glycolysis, mitotic spindle, and MTORC1 signaling were also significantly downregulated, indicating that dip G potentially also has effects on genes related to cancer cell metabolism, cell division, as well as growth factor receptors responsible for ligand-independent activation of ER.

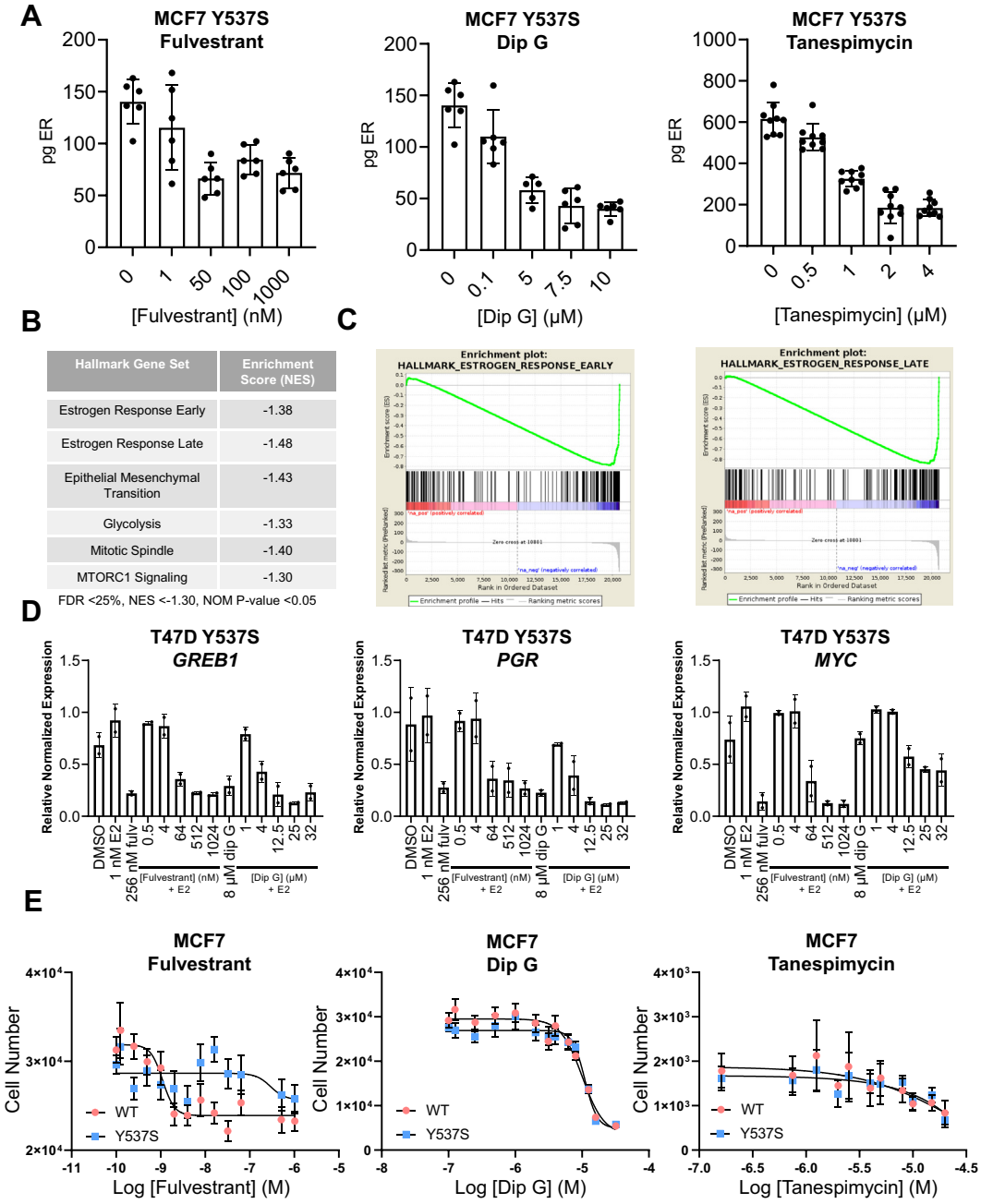

Figure 5. ER Y537S-expressing cells are sensitive to dip G in ER+ cell lines. *A*, ELISA assay of ER levels in MCF7 Y537S cells following treatment with DMSO, 1, 50, 100, and 1000 nM of fulvestrant, with DMSO, 0.1, 5, 7.5, and 10 μM dip G or DMSO, 0.5, 1, 2, and 4 μM tanespimycin for 24 h. MCF7 cells were hormone starved for 3 days prior to treatment. ER protein levels were normalized to 1 x 10^7 cells for fulvestrant and dip G and to total protein concentration for tanespimycin. Two independent experiments with three biological replicates and two technical replicates were carried out for fulvestrant and dip G. Three independent experiments with three biological replicates and two technical replicates were carried out for tanespimycin. Individual biological replicates are plotted. Data are represented as mean ± SD. *B*, hallmark gene set enrichment analysis of significantly changed gene sets (FDR < 25%, NES < -1.3 or NES > 1.3, NOM *p*-value < 0.05) from RNA sequencing of T47D and T47D Y537S cells treated with DMSO or 10 μM dip G for 24 h. One independent experiment with two biological replicates was carried out. *C*, GSEA enrichment plot for hallmark gene set estrogen response early and estrogen response late. *D*, RT-qPCR analysis of ER target gene *GREB1*, *PGR*, and *MYC* expression in T47D Y537S cells treated with DMSO, 1 nM E2, or 1 nM E2 plus increasing concentrations of fulvestrant (0.5–1024 nM) or dip G (1–32 μM) for 24 h. Cells were hormone starved for 3 days prior to treatment. Expression was normalized to *18s rRNA*. Two independent experiments with two biological replicates and three technical replicates were carried out. Individual biological replicates are plotted. Data are represented as mean ± SD. *E*, cell counting data of MCF7 (*pink*) or MCF7 Y537S (*blue*) cells treated for 3 days with increasing concentrations of fulvestrant (0.25–512 nM) dip G (0.5–16 μM) or tanespimycin (0.625–20 μM) in full medium, using a BioTek Lionheart automated microscope. Shown are the number of cells present on the final day of treatment plotted in response to the log of the molar concentration of fulvestrant. Three independent experiments with eight biological replicates were carried out. Data are represented as mean ± SD. dip G, diptoindonesin G; ER, estrogen receptor; GSEA, Gene Set Enrichment Analysis; FDR, false discovery rate.

We validated downregulation of several ER target genes including *GREB1*, *PGR*, and *MYC* in T47D Y537S cells treated with increasing concentrations of fulvestrant and 1 nM E2, as a positive control, or dip G with 1 nM E2 using RT-qPCR, as previously performed for T47D (Fig. 1*E*). In T47D Y537S cells, basal levels of *GREB1*, *PGR*, and *MYC* were 1.5- to 2-fold

higher than in T47D WT cells (Fig. 5*D*). E2 treatment only resulted in a marginal increase in *GREB1*, *PGR*, and *MYC* transcript, respectively, compared to DMSO treatment, consistent with the mutant receptor's constitutively active phenotype and reduced binding to E2 (Fig. 5*D*). This is in contrast to T47D WT cells, where E2 upregulated *GREB1*, *PGR*, and *MYC* expression almost 3.8-fold, 2-fold, and 3.2-fold, respectively, compared to DMSO (Fig. 1*E*). Increasing concentrations of dip G and 1 nM E2 or increasing concentrations of fulvestrant and 1 nM E2 resulted in a dose-dependent decrease in *GREB1, PGR*, and *MYC* expression (Fig. 5*D*).

To test whether inhibition of cell growth correlated with the observed downregulation of ER protein and ER transcriptional activity, MCF7 and MCF7 Y537S cells were treated with increasing concentrations of fulvestrant or dip G in full medium, and cell number was counted for 3 days. We observed a dose-dependent decrease in cell number as the concentration of fulvestrant increased in WT MCF7 cells. ER Y537S cells were less responsive to fulvestrant treatment. WT ER and ER Y537S cells respond almost identically to dip G treatment, as well as tanespimycin treatment, and this response is dose-dependent (Fig. 5*E*). Inhibition of cell growth is correlated with the reduced ER protein levels and ER transcriptional activity, indicating that dip G's antiproliferative effects may be mediated primarily through ER degradation in breast cancer cells. The inhibition of cell growth could be due to cell death, a decrease in cell proliferation, or both. Reports from our own lab, as well as others, have previously reported that dip G does not induce caspase-dependent apoptosis, necroptosis, or autophagic cell death and induces cell cycle arrest at G2/M[45]. In the case of tanespimycin, inhibition of cell growth is not correlated to protein downregulation, and additional effects other than ER degradation, such as downregulation of other protein clients, and induction of apoptosis might better explain tanespimycin's potent antiproliferative effects.

Dip G inhibits PDXO growth and signaling

Given that dip G and tanespimycin inhibited 2D cell proliferation, we next examined whether dip G and tanespimycin could inhibit the growth of PDXOs. To test this, we used HCI-011 PDXOs, which express WT ER but were derived from a patient refractory to treatment (59). HCI-011 PDXOs were treated with DMSO, 10 μM dip G, 1 μM tanespimycin, or 1 μM fulvestrant for 2 weeks. Phase contrast microscopy showed that, in general, organoids in the treated groups were smaller than those in the DMSO-treated group (Fig. 6*A*). In addition, dip G, tanespimycin, and fulvestrant all significantly decreased PDXO viability compared to DMSO treatment, as measured by MTS assay (Fig. 6*B*). RT-qPCR analysis showed significant downregulation of ER target gene *GREB1* in response to dip G and fulvestrant treatment, though tanespimycin had little effect on *GREB1* expression (Fig. 6*C*). We also observed downregulation of ER protein in PDXOs by Western blot in response to dip G and fulvestrant treatment, but not by tanespimycin, indicating that HCI-011 PDXOs rely heavily on ER for growth, and a decrease in viability correlates with ER degradation in dip G and fulvestrant-treated conditions (Fig. 6, *D* and *E*). The cell death caused by tanespimycin could be attributed to the strong cytotoxic effect of this compound rather than targeting ER.

Discussion

In this study, we uncovered that dip G is a small molecule modulator of HSP90 that directly acts on the middle domain of HSP90, rather than the E3 ligase CHIP, as we originally hypothesized (Fig. 3*K*). Dip G promoted WT and mutant ER degradation with similar efficacy (Fig. 5*A*) and inhibited ER-dependent transcription (Fig. 5*D*), thereby eliciting anticancer effects in breast cancer cells expressing ER LBD mutation Y537S (Fig. 5*E*). However, these mutants are somewhat resistant to fulvestrant, as measured by these same end points (Fig. 6*F*).

CHIP is not required for dip G's mechanism of action

Though CHIP may be one of the primary E3 ligases that mediates dip G–induced ER degradation, it is not required for dip G's mechanism of action. When CHIP was knocked out, ER was still degraded in response to dip G (Figure 2, *E* and *F*). One explanation for the discrepancy between our current hypothesis and the model proposed by Zhao *et al.* (43) are the cell lines used. ER is endogenously expressed in MCF7, whereas HS578T-ER-LUC cells are a triple negative breast cancer cell line that expresses exogenously introduced exogenously expresses ER. This may be why depletion of CHIP abrogates dip G–induced ER degradation, as the protein degradation machinery present in MCF7 for degrading ER does not exist in HS578T. We found that expression of CHIP, MDM2, and E6AP, three well-known E3 ligases involved in regulating ER stability, was low in HS578T but high in MCF7 (Fig. S2A). Perhaps, other E3 ligases can compensate in the absence of CHIP in MCF7 but not in HS578T. Results from Mao *et al* showed that manipulating CHIP levels affected prostate cancer cell's sensitivity to dip G (47). This further emphasizes that reliance on CHIP varies between cell lines and cancer types. Our results agree with the results from Fan *et al* (27). Using MCF7, they observed ER degradation in response to geldanamycin treatment when CHIP is knocked down, but the rate of degradation was decreased (27). Functional redundancy is expected, as E3 ligases are important for regulating proteostasis (60). Others have shown that in CHIP null mouse embryonic fibroblasts (MEFs), HSP90 client glucocorticoid receptor could still be degraded at the same rate in response to geldanamycin treatment, indicating that other redundant E3 ligases are likely involved in client stability in the absence of CHIP (60). In agreement with this hypothesis, Fan *et al* showed that multiple E3 ligases colocalize with CHIP at poly Q-expanded AR (27).

Dip G is a middle domain modulator of HSP90

Our data supports that dip G is an HSP90 modulator (Fig. 3*D*). Fluorescence polarization assays confirmed that deoxy-dip G indeed directly binds to HSP90 with an affinity

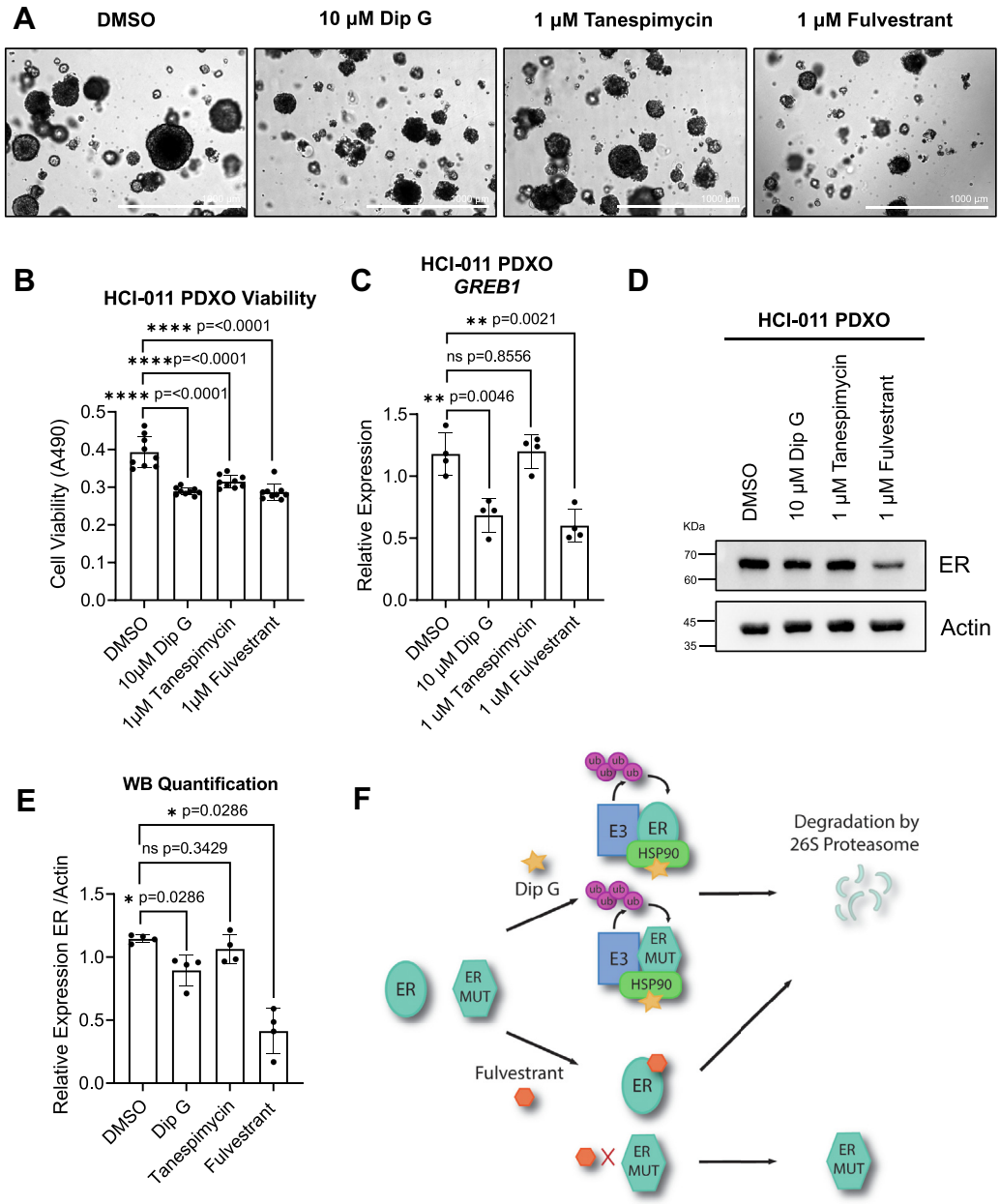

Figure 6. Dip G is effective in a patient-derived xenograft organoid model of ER+ breast cancer. *A*, phase contrast microscopy images of HCI-011 PDXOs treated for 2 weeks with DMSO, 10 μM dip G, 1 μM tanespimycin, or 1 μM fulvestrant in full medium. The scale bar corresponds to 1000 μm. Three biological replicates were carried out with 12 pictures/replicate. One representative image is shown. *B*, MTS data of HCI-011 PDXOs treated for 2 weeks with DMSO, 10 μM dip G, 1 μM tanespimycin, or 1 μM fulvestrant in full medium. Three independent experiments with three biological replicates and three technical replicates were carried out. Plotted are individual biological replicates. Data are represented as mean ± SD. Significance was determined using an unpaired Mann Whitney U test. *C*, RT-qPCR of ER target gene *GREB1* in HCI-011 PDXOs treated with DMSO, 10 μM dip G, 1 μM tanespimycin, or 1 μM fulvestrant in full medium. Expression was normalized to *18s rRNA*. Three independent experiments with three technical replicates were carried out. Individual biological replicates are plotted. Data are represented as the mean ± SD. Significance was determined using an unpaired Mann Whitney test. *D*, Western blot of ER in HCI-011 PDXOs treated with DMSO, 10 μM dip G, 1 μM tanespimycin, or 1 μM fulvestrant in full medium for 3 days. Actin was used as a loading control. Four independent experiments with four biological replicates were carried out. One representative blot is shown. *E*, quantification of the Western blot shown in (D) individual biological replicates are plotted. Data are represented as the mean ± SD. Significance was determined using an unpaired Mann Whitney test. *F*, summary of key data. Dip G promotes ER degradation through the 26S proteasome. CHIP is not required for dip G–mediated ER degradation. Dip G binds to the M-domain of HSP90, which is required for dip G–mediated ER degradation. Y537S mutants are sensitive to dip G and HSP90 inhibitors, but resistant to fulvestrant. dip G, diptoindonesin G; ER, estrogen receptor; HSP90, Heat shock protein 90; PDXO, patient-derived xenograft organoid.

comparable to geldanamycin, an amino-terminal HSP90 inhibitor (Fig. 3*B*, Fig. S3C). We also found that tanespimycin interferes with dip G and deoxy-dip G's ability to induce ER degradation, indicating that they share protein targets (Fig. 3, *I* and *J*, Fig. S3, *K* and *L*). In addition, deoxy-dip G could not be competed off of HSP90 by compounds that bind to the N-terminus, such as geldanamycin (Fig. S3E) and radicicol (Fig. S3G). Deoxy-dip G also could not be competed off by compounds that bind to the C-terminus, including GTP (Fig. S3H), novobiocin (Fig. S3I), and EGCG (Fig. S3J),

supporting that dip G is a middle domain modulator, as it neither competitively binds to N- nor C-termini. However, ATP could compete off deoxy-dip G (Fig. S3F). HSP90 has two reported ATP-binding sites localized in the N- and C-domains. It is possible that ATP induces HSP90 conformational changes by binding to the N or C domains, masking the deoxy-dip G–binding site in the M-domain. HSP90 β middle domain inhibitor sulfoxythiocarbamate acetate also does not inhibit ATP binding (61), which would be consistent with HSP90 binding to ATP in the presence of deoxy-dip G.

Nevertheless, when comparing dip G with HSP90 N-terminal inhibitors like tanespimycin and geldanamycin, there were many similarities. For example, they both bind to HSP90 with high affinity. Many cell lines are sensitive to dip G and tanespimycin. We found that hematologic cancers, in particular, were sensitive to dip G, which agrees with the observations from Gao *et al* (45) (Fig. S4). In breast cancer cell lines, although dip G treatment decreased proliferation of ER+ cells, in keeping with ER degradation, dip G sensitivity did not correlate with ER receptor status, indicating that ER degradation alone does not explain dip G's antiproliferative effects, consistent with dip G being an HSP90 inhibitor (Fig. S4). Among breast cancer cell lines, MDA-MB-231 was particularly sensitive to dip G (Fig. S4), which is consistent with observations from Fan *et al* (46). In addition, both dip G and tanespimycin affect a variety of proteins, many of which are known HSP90 clients (Table S2). However, when comparing their respective affected proteomes, we found that though there was some overlap between tanespimycin and dip G–affected proteins, about 51% of the proteins upregulated by dip G and 70% of the proteins downregulated by dip G were unique, indicating that dip G has a distinct mechanism of action from tanespimycin even though the compounds share some targets (Figure 4, *D* and *E*). The distinction between dip G and other HSP90 inhibitors is further emphasized by dip G, tanespimycin, and novobiocin's induction of HSR, where tanespimycin was the only compound to significantly increase the levels of all HSPs (Fig. 3*H*), consistent with what has been previously reported. We believe that only tanespimycin induces HSR because binding of N-terminal ATP competitive inhibitors to HSP90 interferes with HSP90-HSF1. HSF1 is normally sequestered by HSP70 and HSP90, preventing HSF1 from initiating transcription of HSR genes. Dip G likely does not interfere with HSP90–HSF1 interaction (62, 63).

HSP90 is required for transcription-coupled ER degradation. However, as mentioned previously, degradation can be coupled to both transcriptional activation, as well as transcriptional repression, and can be explained by ER being regulated by two different ubiquitin proteasome pathways, depending on whether ER is liganded (64). One proteasome is responsible for the transactivation of ER, while the other proteasome is responsible for ER quality control (64). Tateishi *et al.* showed using MEFs that under thermally stressed conditions, unliganded ER was degraded in CHIP-expressing MEFs, but not in CHIP null MEFs, whereas in both CHIP-expressing and CHIP-null MEFs, ER was degraded in the presence of estrogen (64).

Although both dip G and tanespimycin promote ER degradation engaging HSP90, their mechanisms of action differ. Dip G appears to stabilize the HSP90–E3–ER complex, promoting ER degradation, whereas tanespimycin binding to HSP90 promotes dissociation of ER and causes ER misfolding and subsequent degradation. When tanespimycin and dip G were cotreated in cells with E2, they behaved very differently. Cotreatment of E2 and tanespimycin stabilized receptor levels compared to tanespimycin alone, which promoted ER degradation (Fig. 3, *I* and *J*). This is likely because some ER is already bound to ligand and is no longer complexed with HSP90, and some HSP90 is bound to tanespimycin, inhibiting ER's hormone-binding ability. E2 and dip G have an additive effect on ER degradation, indicating that dip G can promote degradation of activated ligand-bound ER and that dip G likely engage other mechanisms to destroy ER and promote degradation of transcription-coupled ER, unlike tanespimycin, which could not promote degradation of ligand-bound ER (Fig. 3, *I* and *J*). Dip G can promote degradation of certain ligand-stabilized ERs, such as E2 treated, but not OHT-treated ER (Fig. 3, *I* and *J*). This would support a mechanism where dip G can only promote degradation of HSP90-bound ER and cannot degrade ER on chromatin, which is why residual levels of ER are still observed by Western blot. However, tanespimycin and dip G do not affect fulvestrant-mediated degradation, where degradation is independent of ER transcription (Fig. 3, *I* and *J*). Instead, fulvestrant immobilizes ER to the nuclear matrix, where it can then be degraded (65). When dip G and tanespimycin coexist, tanespimycin offsets the effect of dip G, and less HSP90–E3–ER complex could form. Even though these two compounds do not compete for the same sites on HSP90, they compete for the same pool of HSP90, and binding of one may prohibit the binding of the other, resulting in the higher amount of ER observed compared to either treatment alone. Another explanation is that, rather than compete for sites on HSP90, both compounds can bind to HSP90 simultaneously but antagonize the effect of the other, resulting in ER stabilization rather than additive ER degradation.

Our most striking evidence supporting dip G as an M-domain modulator is that deoxy-dip G bound with highest affinity to a fragment corresponding to the middle domain of HSP90 to a much greater extent than either the N or C fragments of HSP90 (Fig. 3, *D–F*). To our knowledge, only a handful of middle domain inhibitors have been reported. Kongensin A binds covalently to the middle domain of HSP90 at cysteine 420. Binding to C420 disrupts the association between HSP90 and CDC37, a cochaperone of HSP90 that not only provides specificity for HSP90's interactions with client proteins, but also activation of kinase clients (66). This residue is essential for kongensin A's mechanism as the interaction between HSP90 and CDC37 was restored when C420 was mutated to an alanine (66). The methods we used in our study can only pinpoint dip G's binding between AA 272-617. Kongensin A can also promote degradation of HSP90 client proteins such as HER2, AKT, and B-RAF (66). Another HSP90 M-domain ligand triptolide is selective for the HSP90 β isoform and blocks the interaction of HSP90 and CDC37, but

through binding to C366 (67). Gambogic acid and sulfoxythiocarbamate acetate has also been reported as selective for the middle domain of the HSP90 β isoform (61, 68) Other HSP90 inhibitors have been reported to allosterically inhibit HSP90–cochaperone interactions, such as withaferin A (69), celastrol (70), derrubone (71), but they have not been reported to bind to the M-domain of HSP90.

Dip G not only has therapeutic applications in cancer but is also a probe to better understand HSP90 middle domain biology. Specifically, dip G could be used to break down part of HSP90's conformational equilibrium and conformation cycle. This is because the middle domain is not only involved in client protein and cochaperone binding but also can modulate the ATPase activity of the N-domain by binding ATPase-stimulating cochaperone AHA1 (72).

HSP90 inhibition can overcome endocrine resistance in breast cancer

Dip G could promote mutant ER degradation in ER+ breast cancer cells (Fig. 1*D*) and elicited antiproliferative effects (Fig. 5*E*). We also performed many *in vivo* studies using dip G and deoxy-dip G in several different models of ER+ breast cancer, including patient-derived xenograft models. However, we found that dip G and deoxy-dip G had no significant effect on tumor growth (data not shown). One explanation for the discrepancy between our *in vitro* and *in vivo* results is that therapeutic concentrations of dip G could not be reached in a mouse due to physical and drug solubility limitations. To circumvent these limitations, we instead utilized an organoid system derived from one of the PDXs used in our *in vivo* studies and treated them using our 2D culture conditions (Fig. 6*A–D*). Others have found that dip G has antitumor effects *in vivo* using models that are more sensitive to dip G, such as MDA-MB-231 xenografts (46), consistent with our PRISM analysis. Testing the effects of dip G in an ER Y537S-expressing PDXO model to complement our HCI-011 PDXO results warrants further investigation.

Using HSP90 inhibitors to treat endocrine-resistant breast cancer has not been extensively explored. Toy *et al.* treated MCF7 cells transfected with vector expressing HA-tagged WT ER or Y537S and D538G mutant ER with SNX2112, an N-terminal ATP-binding site–targeting drug, at various doses for 3 h (3). Though WT ER levels were decreased in a dose-dependent manner, HSP90 inhibition did not affect the levels of Y537S and D538G mutant ER, indicating that HSP90 does not regulate mutant ER stability (3). On the contrary, Yu *et al.* found that ganetespib had cytotoxic effects in *ex vivo*–cultured circulating tumor cells expressing *ESR1* mutations as a single agent but also in combination with raloxifene and fulvestrant (73). They also found that sensitivity to HSP90 inhibition was associated with mutant *ESR1* allele frequency (73). Though the Y537S mutant resembles E2-bound ER in phenotype and structure, we found that ER mutant protein can be degraded in response to both dip G and tanespimycin treatment (Fig. 5*A*), indicating that the Y537S mutant, and perhaps other LBD mutants, still associate and rely on HSP90. Because the conclusions of Toy *et al.* conflict with the results from Yu *et al*, as well as our own results, where we found that efficacy of HSP90 inhibition is not affected by ER mutational status, further mechanistic studies are required to determine conclusively whether HSP90 associates with mutant ER and whether this phenomenon holds true for other classes of N-terminal–, as well as C-terminal–targeting HSP90 inhibitors. Establishing definitively whether HSP90 can interact with *ESR1* LBD mutants could open up a new class of drug for treatment of mutant-ER–expressing tumors and help better understand the biology of *ESR1* LBD mutants.

We propose a new hypothesis for dip G–induced ER degradation, implicating HSP90 as dip G's direct target. We also provide additional insight on understanding of ER degradation mechanisms and the biology of HSP90 inhibition and propose a new therapeutic strategy for treating endocrine-resistant breast cancer that has yet to be fully explored.

Experimental procedures

2D cell culture

MCF7, LCC-2, and BT474 cells were all purchased from the American Type Culture Collection (ATCC). MCF7 WT and MCF7 Y537S cells were provided by Dr. Ben Ho Park. T47D WT and T47D Y537S cells were provided by Dr. Shunqiang Li. All MCF7 cell lines were maintained in Dulbecco's modified Eagle's medium (DMEM) supplemented with 10% FBS (Gibco) and 1% penicillin-streptomycin. T47D cell lines were maintained in RPMI 1640 (Gibco) supplemented with 10% FBS, 1% penicillin-streptomycin, 1% HEPES, 1% L-glutamine, and 1% sodium pyruvate. For subculturing for all experiments, MCF7 and T47D cell lines were all seeded in full medium. The following day, cells were washed with Dulbecco's phosphate-buffered saline and medium was changed to phenol red–free equivalents of the culture conditions described above with the substitution of 5% 6X charcoal-stripped FBS. MCF7 and T47D cells were hormone starved for 3 days prior to using in all experiments, with the exception of T47D cells used for RNA-seq, which were only hormone starved for 24 h. For measuring HSR, cells were cultured in full medium. All cells were cultured at 37 °C in a humidified incubator at 5% CO_2.

Generation of LCC-2 CHIP KD cell lines

LCC-2 shControl and shCHIP cell lines were generated as previously described for MCF7 shControl and shCHIP cells (43).

Generation of CHIP KO cell lines

To generate the MCF7 KO cell lines, a guide RNA (sense 5′ AAACACTGCCGGCGCGCCCTGGAGC 3′, antisense 5′CAC CGCTCCAGGGCGCGCCGGCAGT 3′) specifically targeting exon 2 of *STUB1* was designed, and cloned into a CRISPR/Cas9/eGFP plasmid PX458 (Addgene, #48138), and sequenced as previously described (49). Cells were transfected using TransIT-LT1 transfection reagent (Mirus, CAT# MIR 2306) according to the manufacturer's instructions. Forty eight hours following transfection, cells were sorted using a BD FACSAria

cell sorter at the UW Carbone Cancer Center Flow Cytometry Laboratory, selecting only cells expressing high levels of GFP. Sorted cells were seeded as single cells into 96-well plates and were allowed to form colonies for approximately one month, and medium was refreshed weekly. Colonies were expanded and screened individually by Western blot.

Western blot

Proteins were resolved by SDS-PAGE and were transferred to nitrocellulose membranes using the Bio-Rad Turbo Blot (Bio-Rad). Blots were blocked with 5% nonfat milk in PBS with 0.1% tween 20 (PBST) for 1 to 2 h at room temperature on a shaker and then incubated with primary antibodies diluted in 5% nonfat milk in PBST at 4 °C overnight on a rotator. The primary antibodies and dilutions used in this study are as follows: estrogen receptor α F-10 (Santa Cruz Biotechnology. CAT# sc-8002, 1:2,000), CHIP H-231 (Santa Cruz Biotechnology. CAT# SC-66830, 1:1,000), HSP90 α/β H-114 (Santa Cruz Biotechnology. CAT# SC-7947, 1:1,000), ubiquitin P4D1 (Santa Cruz Biotechnology CAT# SC-0817, 1:1,000), MDM2 (Cell Signaling Technology. CAT#86934S, 1:1,000), HER2 (Cell Signaling Technology. CAT#2165S, 1:1,000), E6AP (Invitrogen. CAT# 703785, 1:500), β-actin (Sigma, CAT#A5441, 1:5,000). Blots were washed for 30 min in PBST and then incubated with a goat anti-rabbit (Jackson ImmunoResearch, CAT# 111-035-144, 1:5,000) and goat anti-mouse (Jackson ImmunoResearch. CAT# 115-035-062, 1:5,000) horse radish peroxidase–labeled secondary antibodies diluted in 5% nonfat milk in PBST for 1 to 2 h at room temperature. Blots were washed once for 30 min on a shaker in PBST and incubated with SuperSignal West Pico ECL (Thermo Fisher Scientific) prepared according to the manufacturer's instructions. Blots were exposed using a Bio-Rad ChemiDoc (Bio-Rad).

Mass spectrometry

Protein extraction and trypsin digestion

The lysis buffer containing 8M urea and protease and phosphatase inhibitors were added into biological samples at a 1:10 (w/v) ratio. Samples were placed on ice and sonicated 1 min with a 3-s interval at amplitude 25%. Then, the lysate was reduced with 10 mM DTT at 37 °C for 1 h and alkylated with 20 mM iodoacetamide at room temperature in the dark for an additional 15 min. BCA assay (Thermo Fisher) was performed to determine the proteins concentration and around 100 μg of protein was then digested using trypsin at an enzyme to protein ratio of 1:100 (w/w) at 37 °C overnight. Digested peptides were desalted using C18 cartridges (Waters) and dried in SpeedVac. The concentrations of peptide mixture were measured by peptide assay (Thermo Fisher). Samples were lyophilized and stored at −80 °C.

Liquid chromatography-tandem mass spectrometry analysis

The liquid chromatography-tandem mass spectrometry analysis was performed on a Q Exactive HF mass spectrometer (Thermo Fisher) coupled to a nanoflow HPLC (Dionex UltiMate 3000 UPLC system, Thermo Fisher) with a nanoelectrospray ion source (Thermo Fisher). Peptides were reconstituted in 0.1% formic acid (FA) and about 0.5 μg of peptides were loaded onto a 75 μm × 15 cm self-fabricated column packing with 1.7 μm Ethylene Bridged Hybrid packing materials (130 Å, Waters). A 126-min linear gradient of 3 to 45% mobile phase B (buffer A, 0.1% FA in water; buffer B, 0.1% FA in ACN) at a flow rate of 0.3 μl/min. The MS analysis was performed in a data-dependent manner using an Orbitrap mass analyzer. For a full mass spectrometry survey scan, the automatic gain control value was 1e5, and the scan ranged from 300 to 2000 m/z at a resolution of 60,000, with a maximum injection time of 100 ms. For the MS2 scan, up to 15 of the most intense precursor ions from a survey scan were selected for MS/MS and detected by the Orbitrap at a mass resolution of 15,000 at m/z 400. Only spectra with a charge state of 2–6 were selected for fragmentation by higher-energy collision dissociation with normalized collision energy of 30%. The automatic gain control for MS/MS was set to 8e3, with maximum ion injection times of 100 ms. Dynamic exclusion time was 30 s, and the isolation window of the precursors was 1.4 Th.

Label-free–based MS quantification for proteins

MaxQuant (version 1.5.3.8) with the integrated Andromeda search engine was used for database searching and protein identification and quantification. The false discovery rate was controlled below 1% at both peptide and protein level. The tandem mass spectra were searched against the human UniProt database (version 20200219, 20,193 sequences). A reverse database for the decoy search was generated automatically in MaxQuant. Trypsin was selected as the enzyme in specificity, and a minimum number of seven amino acids were required for peptide identification. For label-free protein quantification (LFQ), the MaxQuant LFQ algorithm was enabled to quantitate the MS signals, and the proteins' intensities were represented in LFQ intensity. Cysteine carbamidomethylation was set as the fixed modification, and methionine oxidation as well as protein N-terminal acetylation were set as the variable modifications. The first search mass tolerance was set as 20 ppm, and the main search peptide tolerance was 4.5 ppm. The false discovery rate of the peptide-spectrum matches and proteins were set to less than 1%.

ELISA

Cells were seeded in 6-cm dishes in full medium. Following hormone starvation, cells were treated with drug (see related figures for drug treatments and concentrations) for 24 h. Cells were trypsinized and collected. ELISA was performed using a Human Total ER alpha/NR3A1 DuoSet IC ELISA (R&D Systems) following the manufacturer's instructions.

Fluorescence polarization

To measure binding to full length HSP90, as well as HSP90 fragments, deoxy-dip G (final concentration of 1 μM) was mixed with a serially diluted concentrations of protein in In Black Nunc 384-Shallow Well Standard Height Polypropylene

Microplates (Catalog Number: 267461) in 50 mM HEPES, 75 mM NaCl, 0.01% Triton X-100, pH 7.4, with a final assay volume of 20 μl. After mixing, the plate was incubated at room temperature for 20 min. The polarization signals (mP) were acquired by PHERAstar FS Plate Reader (FP 485-520–520 nM Optic module). K_d and IC_{50} were calculated using GraphPad 6.0. The competition assays were performed as described for the binding assays to HSP90, but competing protein concentrations were kept constant and competed with serially diluted competitor.

HSP90 fragment expression and purification

Purified GST-Hsp90 N (9-236) (Addgene #22481), GST-Hsp90 M (272-617) (Addgene #22482), and GST-Hsp90 C (626–-732) (Addgene #22483) plasmids were transformed into BL21 cells and used to inoculate a 5 ml starter cultures in LB with ampicillin grown overnight at 37 °C in a shaker. The following day, the starter cultures were used to inoculate 500 ml LB with ampicillin, which were grown at 37 °C in a shaker. When the A600 nM reached 0.8 to 1, cultures were treated with 1M IPTG (1:500) and were placed in a shaker overnight at room temperature. The following day, cultures were spun down at 4 °C at 13,000 rpm. The supernatant was decanted and the pellets were stored at −20 °C until use. The pellet was thawed on ice and sonicated (30 s on 30 s off 50% amplitude for 5 min) in 15 ml of lysis buffer (25 mM Tris pH 7.5, 1 mM EDTA, 157 mM NaCl, 1% Triton X-100, and protease inhibitor cocktail) on ice. Lysate was spun down at 13,000 rpm at 4 °C for 20 min. 0.5 mL of Glutathione Agarose Resin (Pierce) were washed once with 10 ml of lysis buffer and loaded with lysate supernatant and incubated on a rotator overnight at 4 °C. Beads were washed with 10 ml of wash buffer I (25 mM Tris pH 7.5, 2 mM EDTA, 500 mM NaCl, 0.5% NP-40, and protease inhibitor cocktail) and then 10 ml of wash buffer II (53 mM Tris pH 8, 1 mM EDTA, 157 mM NaCl, 10% glycerol, and protease inhibitor cocktail). Beads were then washed twice with 12 ml of thrombin cleavage buffer (2.5 mM Tris pH 8, 3 mM NaCl, 6.25 μM $CaCl_2$, 4 μM DTT). The beads were transferred to microcentrifuge tubes and spun down at 2000 rpm for 20 s. The supernatant was removed, and the beads were resuspended in 2X the bead volume of thrombin cleavage buffer. Two units of thrombin enzyme (Novogen) was added/100 μL of beads. The tubes were incubated on a rotator at room temperature for 30 min. The tubes were then spun down at 2000 rpm for 20 s and transferred to a new tube (elution 1). An addition 2X the bead volume of thrombin cleavage buffer was added and incubated on a rotator for 5 min. The tubes were spun down at 2000 rpm for 20 s and the supernatant was transferred to a new tube (elution 2).

Coomassie Blue staining

SDS-PAGE gel was removed from the electrophoresis chamber and placed in enough Coomassie Blue G-250 solution (prepared in 50% methanol, 10% acetic acid) to cover the gel. Gel was stained for 5 min. Stain was discarded, and the gel was rinsed with distilled water to remove residual stain and destained with destaining solution (40% methanol, 10% acetic acid) for 20 min. Destaining solution was removed, and gel was destained in distilled water overnight.

PRISM

The PRISM assay was performed as previously described (56).

RNA-seq

RNA was extracted from T47D WT and T47D Y537S cell pellets using the ENZA Total RNA Extraction Kit (Omega) following the manufacturer's instructions. RNA-seq libraries were prepared using the Illumina TruSeq RNA Library Prep Kit v2 following the manufacturer's instructions. Each library was sequenced in single read mode, 1 × 50 bp, using the HiSeq4000 platform. Sequencing reads were aligned to human genome (hg38 assembly) using STAR (74). Read counts were performed using HTSeq (75). Differentially expressed genes were identified by DESeq2 (76) under where a significantly changed gene experienced at least a 1.5-fold change and had an adjusted p-value < 0.05. GSEA (77, 78), using hallmark gene sets, was performed by taking the total detected genes with $p < 0.05$ in the T47D Y537S dip G treatment versus T47D Y537S DMSO treatment.

RT-qPCR

Total cellular RNA was extracted from cell lines and organoids using the ENZA Total RNA Kit (Omega) according to the manufacturer's instructions. 1 μg of RNA was reverse transcribed using Superscript II RT (Invitrogen). Quantitative PCR was performed using SYBR Green Master Mix (Roche Scientific) per the manufacturer's instructions (including cycling parameters) and the BioRad CFX96 Touch Real-Time PCR Detection System (BioRad). The Cq values obtained for the genes of interest were then normalized to the the respective Cq values of *18s rRNA*.

18s rRNA Forward: TAGTAGCGACGGGCGGTGTG
Reverse: CAGCCACCCGAGATTGAGCA
GREB1 Forward: GTGGTAGCCGAGTGGACAAT
Reverse: ATTTGTTTCCAGCCCTCCTT
PGR Forward: GGCCAGCAGTCCTGCAACAGTC
Reverse: CCCAAGCTTGTCCGCAGCCTT
HSP27 Forward*:* AAGCTAGCCACGCAGTCCAA
Reverse: CGACTCGAAGGTGACTGGGA
HSP40 Forward*:* GGACTATGGACTCTTTCAAAGG
Reverse: GTAATCAGAAGCAAAGACCC
HSP70 Forward: ATGTCGGTGGTGGGCATAGA
Reverse: ACAGCGACGTAGCAGCTCT
HSP90 Forward: GAAATCTGTAGAACCCAAATTTCAA
Reverse: TCTTTGGATACCTAATGCGACA

Cell counting

3×10^3 cells/well were seeded in 100 μl of medium, according to the cell line's culture conditions, in 96-well plates. The next day, 100 μl of 2X concentrated drugs diluted in medium were added to each well. Drugs and medium were

refreshed every day for 3 days. Cells were imaged and counted every day on the Lionheart FX Automated Microscope (Bio-Tek) at 37 °C.

3D organoid culture

Organoids were cultured as previously described (59). Briefly, organoids were embedded in Matrigel (Corning) domes in a multi-well plate. For a 96-well plate, 30 to 40 μL of Matrigel and organoids were used. For a 24-well plate, 40 μL of Matrigel and organoids was used. Plates were flipped and incubated for 30 min at 37 °C to allow Matrigel to solidify and reduce the number of organoids growing on plastic. Following the 30 min incubation, medium was added. Organoids were maintained in advanced DMEM supplemented with 5% FBS, 1% penicillin streptomycin, HEPES, Glutamax, gentamycin, 10 ng/ml human epidermal growth factor (EGF), 1 μg/ml hydrocortisone, 100 ng/ml fibroblast growth factor 2 (FGF2), 1 mM N-Acetyl-L-cysteine, and fresh 10 μM Y-27632. Media was exchanged every 3 to 4 days. Mature cultures were passaged using cell recovery solution according to the manufacturer's instructions, followed by dissociation in TrypLE (Gibco) for 10 to 15 min at 37 °C, with occasional shaking, to dissociate organoids into single cells and smaller organoids.

Cell titer 96 AQueous one solution cell proliferation assay

Organoids were seeded and cultured as described above. The next day, organoids were treated with drugs. Drugs and medium were refreshed every day for 2 weeks. The proliferation assay was performed according to the manufacturer's instructions (Promega).

Statistical analysis

Biological replicates from at least three independent experiments were used to perform statistical analyses. The number of technical and biological replicates and independent experiments is listed in each figure legend. A Shapiro-Wilk test was performed to determine whether data follow a normal (Gaussian) distribution. To determine whether the difference between the two means is significant for data that follow a normal distribution, a parametric unpaired *t* test with Welch's correction was performed. For data that do not follow a normal distribution, a nonparametric Mann-Whitney test was used. Exact *p*-values are listed in each figure or figure legend. A p-value > 0.05 is considered significant. For RNA-seq, significantly upregulated or downregulated genes are defined as genes that are changed at least 1.5-fold and have a p-value > 0.05 with a false discovery rate less than 25%. For proteomics data, significantly upregulated or downregulated proteins are defined as those that are changed at least 1.5-fold and have a p-value > 0.05.

Data availability

RNA-seq data have been deposited at GEO and are publicly available as of the date of publication at GEO accession number GEO GSE205716. Proteomics data have been deposited at Proteome Xchange and are publicly available as of the data of publication at PXD035398. Any additional information required to reanalyze the data reported in this article is available from the lead contact upon request.

Resource availability

Lead contact

Further information and requests for resources and reagents should be directed to and will be fulfilled by the lead contact, Wei Xu (wxu@oncology.wisc.edu).

Materials availability

All unique and stable reagents generated in this study are available from the lead contact with a completed Materials Transfer Agreement.

Supporting information—This article contains supporting information.

Acknowledgments—HCI PDXO models were a gift from Alana Welm. GST-HSP90 fragment plasmids were a gift from William Sessa (Addgene plasmids #22481, 22482, 22483). The pSpCas9(BB)-2A-GFP (PX458) plasmid was a gift from Feng Zhang (Addgene plasmid # 48138). MCF7 WT and MCF7 Y537S cells were kindly provided by Dr Ben Ho Park. We would also like to thank the UW Carbone Cancer Center Flow Cytometry Core for their assistance with cell sorting.

Author contributions—K. D., H. X., M. L., M. M., L. L., W. T., and W. X. conceptualization; K. D., M. L., M. M., L. L., and W. X. methodology; Y. W., K. D., H. X., M. L., A. G., M. M., Y. W., R. T., N. S., and T. P. investigation; K. D., A. G., R. T., N. S., and T. P. formal analysis; K. D. and W. X. writing–original draft; S. L., L. L., W. T., and W. X. supervision; K. D., M. L., and M. M. data curation; K. D. and H. X. visualization; K. D., H. X., W. T., and W. X. writing–review and editing; M. L. and M. M. resources; S. L., L. L., W. T., and W. X. project administration; W. X. funding acquisition.

Funding and additional information—This work was supported by National Cancer Institute CA236356, National Cancer Institute CA268183-01A1, and Department of Defense W81XWH-20-1-0022 to W. X. and National Research Service Award T32 CA009135 to K. D.

Conflict of interest—W. X. and W. T. are the inventors, and the Wisconsin Alumni Research Foundation is the assignee, on patent number 10508092, "Synthesis of novel analogs of diptoindonesin G, compounds formed thereby, and pharmaceutical compositions containing them". All other authors declare no competing interests.

Abbreviations—The abbreviations used are: dip G, diptoindonesin G; ER, estrogen receptor; FA, formic acid; FBS, fetal bovine serum; GSEA, Gene Set Enrichment Analysis; HSP90, heat shock protein 90; HSR, heat shock response; LBD, ligand-binding domain; LFQ, label-free quantification; MEF, mouse embryonic fibroblast; OHT, hydroxytamoxifen; PBST, PBS with 0.1% tween 20; PDXO, patient-derived xenograft organoid.

References

1. Jeselsohn, R., Buchwalter, G., de Angelis, C., Brown, M., and Schiff, R. (2015) ESR1 mutations-a mechanism for acquired endocrine resistance in breast cancer. Nat. Rev. Clin. Oncol. *Preprint*. https://doi.org/10.1038/nrclinonc.2015.117
2. Robinson, D. R., Wu, Y., Vats, P., Su, F., Lonigro, R., Cao, X., *et al.* (2013) Activating ESR1 mutations in hormone-resistant metastatic breast cancer. *Nat. Genet.* https://doi.org/10.1038/ng.2823
3. Toy, W., Shen, Y., Won, H., Green, B., Sakr, R., Will, M., *et al.* (2013) ESR1 ligand-binding domain mutations in hormone-resistant breast cancer. *Nat. Genet.* https://doi.org/10.1038/ng.2822
4. Jeselsohn, R., Yelensky, R., Buchwalter, G., Frampton, G., Meric-Bernstam, F., Gonzalez-Angulo, A., *et al.* (2014) Emergence of constitutively active estrogen receptor-α mutations in pretreated advanced estrogen receptor–positive breast cancer. *Clin. Cancer Res.* **20**, 1757 LP–1767 LP
5. Li, S., Shen, D., Shao, J., Crowder, R., Liu, W., Prat, A., *et al.* (2013) Endocrine-therapy-resistant ESR1 variants revealed by genomic characterization of breast-cancer-derived xenografts. *Cell Rep*. https://doi.org/10.1016/j.celrep.2013.08.022
6. Merenbakh-Lamin, K., Ben-Baruch, N., Yeheskel, A., Dvir, A., Soussan-Gutman, L., Jeselsohn, R., *et al.* (2013) D538G mutation in estrogen receptor-α: a novel mechanism for acquired endocrine resistance in breast cancer. *Cancer Res.* https://doi.org/10.1158/0008-5472.CAN-13-1197
7. Jeselsohn, R., Bergholz, J., Pun, M., Cornwell, M., Liu, W., Nardone, A., *et al.* (2018) Allele-specific chromatin recruitment and therapeutic vulnerabilities of ESR1 activating mutations. *Cancer Cell*. https://doi.org/10.1016/j.ccell.2018.01.004
8. Fanning, S. W., Mayne, C., Dharmarajan, V., Carlson, K., Martin, T., Novick, S., *et al.* (2016) Estrogen receptor alpha somatic mutations Y537S and D538G confer breast cancer endocrine resistance by stabilizing the activating function-2 binding conformation. *Elife*. https://doi.org/10.7554/eLife.12792
9. Zhao, Y., Laws, M., Guillen, V., Ziegler, Y., Min, J., Sharma, A., *et al.* (2017) Structurally novel antiestrogens elicit differential responses from constitutively active mutant estrogen receptors in breast cancer cells and tumors. *Cancer Res.* https://doi.org/10.1158/0008-5472.CAN-17-1265
10. Katzenellenbogen, J. A., Mayne, C. G., Katzenellenbogen, B. S., Greene, G. L., and Chandarlapaty, S. (2018) Structural underpinnings of oestrogen receptor mutations in endocrine therapy resistance. *Nat. Rev. Cancer* **18**, 377–388
11. Wardell, S. E., Yllanes, A., Chao, C., Bae, Y., Andreano, K., Desautels, T., *et al.* (2020) Pharmacokinetic and pharmacodynamic analysis of fulvestrant in preclinical models of breast cancer to assess the importance of its estrogen receptor-α degrader activity in antitumor efficacy. *Breast Cancer Res Treat*. https://doi.org/10.1007/s10549-019-05454-y
12. van Kruchten, M., de Vries, E., Glaudemans, A., van Lanschot, M., van Faassen, M., Kema, I., *et al.* (2015) Measuring residual estrogen receptor availability during fulvestrant therapy in patients with metas tatic breast cancer. *Cancer Discov.* https://doi.org/10.1158/2159-8290.CD-14-0697
13. Robertson, J. F. R. (2007) Fulvestrant (Faslodex®)—How to make a good drug better. *Oncologist*. https://doi.org/10.1634/theoncologist.12-7-774
14. Robertson, J. F. R., and Harrison, M. Fulvestrant (2004) Pharmacokinetics and pharmacology. *Br. J. Cancer*. https://doi.org/10.1038/sj.bjc.6601630
15. Guan, J., Zhou, W., Hafner, M., Blake, R., Chalouni, C., Chen, I., *et al.* (2019) Therapeutic ligands antagonize estrogen receptor function by impairing its mobility. *Cell*. https://doi.org/10.1016/j.cell.2019.06.026
16. Weir, H. M., Bradbury, R., Rabow, A., Buttar, D., Callis, R., Curwen, J., *et al.* (2016) AZD9496: an oral estrogen receptor inhibitor that blocks the growth of ER-positive and ESR1-mutant breast tumors in preclinical models. *Cancer Res.* https://doi.org/10.1158/0008-5472.CAN-15-2357
17. Lai, A., Kahraman, M., Govek, S., Nagasawa, J., Bonnefous, C., Julien, J., *et al.* (2015) Identification of GDC-0810 (ARN-810), an orally bioavailable selective estrogen receptor degrader (SERD) that demonstrates robust activity in tamoxifen-resistant breast cancer xenografts. *J. Med. Chem.* https://doi.org/10.1021/acs.jmedchem.5b00054
18. Bihani, T., Patel, H. A., rlt, H., Tao, N., Jiang, H., Brown, J., *et al.* (2017) Elacestrant (RAD1901), a Selective Estrogen Receptor Degrader (SERD), has antitumor activity in multiple ER+ breast cancer patient-derived xenograft models. *Clin. Cancer Res.* https://doi.org/10.1158/1078-0432.CCR-16-2561
19. Trepel, J., Mollapour, M., Giaccone, G., and Neckers, L. (2010) Targeting the dynamic HSP90 complex in cancer. *Nat. Rev. Cancer*. https://doi.org/10.1038/nrc2887
20. Grenert, J. P., Johnson, B. D., and Toft, D. O. (1999) The importance of ATP binding and hydrolysis by Hsp90 in formation and function of protein heterocomplexes. *J. Biol. Chem.* **274**, 17525–17533
21. Pratt, W. B., and Toft, D. O. (1997) Steroid receptor interactions with heat shock protein and immunophilin chaperones*. *Endocr. Rev.* **18**, 306–360
22. Kamal, A., Thao, L., Sensintaffar, J., Zhang, L., Boehm, M., Fritz, L., *et al.* (2003) A high-affinity conformation of Hsp90 confers tumour selectivity on Hsp90 inhibitors. *Nature*. https://doi.org/10.1038/nature01913
23. Zhou, W., and Slingerland, J. M. (2014) Links between oestrogen receptor activation and proteolysis: relevance to hormone-regulated cancer therapy. Nat. Rev. Cancer *Preprint*. https://doi.org/10.1038/nrc3622
24. Helzer, K. T., Szatkowski Ozers, M., Meyer, M., Benkusky, N., Solodin, N., Reese, R., *et al.* (2018) The phosphorylated estrogen receptor α (ER) cistrome identifies a subset of active enhancers enriched for direct ER-DNA binding and the transcription factor GRHL2. *Mol. Cell Biol*. https://doi.org/10.1128/mcb.00417-18
25. Deng, L., Meng, T., Chen, L., Wei, W., and Wang, P. (2020) The role of ubiquitination in tumorigenesis and targeted drug discovery. *Signal Transduc. Target. Ther.* https://doi.org/10.1038/s41392-020-0107-0
26. Saji, S., Okumura, N., Eguchi, H., Nakashima, S., Suzuki, A., Toi, M., *et al.* (2001) MDM2 enhances the function of estrogen receptor in human breast cancer cells. *Biochem. Biophys. Res. Commun.* https://doi.org/10.1006/bbrc.2001.4339
27. Fan, M., Park, A., and Nephew, K. P. (2005) CHIP (carboxyl terminus of Hsc70-interacting protein) promotes basal and geldanamycin-induced degradation of estrogen receptor-α. *Mol. Endocrinol.* https://doi.org/10.1210/me.2005-0111
28. Hashizume, R., Fukuda, M., Maeda, I., Nishikawa, H., Oyake, D., Yabuki, Y., *et al.* (2001) The RING Heterodimer BRCA1-BARD1 is a ubiquitin ligase Inactivated by a breast cancer-derived mutation. *J. Biol. Chem.* https://doi.org/10.1074/jbc.C000881200
29. Eakin, C. M., MacCoss, M. J., Finney, G. L., and Klevit, R. E. (2007) Estrogen receptor α is a putative substrate for the BRCA1 ubiquitin ligase. *Proc. Natl. Acad. Sci. U S A*. https://doi.org/10.1073/pnas.0610887104
30. Bhatt, S., Xiao, Z., Meng, Z., and Katzenellenbogen, B. S. (2012) Phosphorylation by p38 mitogen-activated protein kinase promotes estrogen receptor turnover and functional activity via the SCFSkp2 proteasomal complex. *Mol. Cell Biol*. https://doi.org/10.1128/mcb.06561-11
31. Sun, J., Zhou, W., Kaliappan, K., Nawaz, Z., and Slingerland, J. M. (2012) ERα phosphorylation at Y537 by Src triggers E6-AP-ERα binding, ERα ubiquitylation, promoter occupancy, and target gene expression. *Mol. Endocrinol.* https://doi.org/10.1210/me.2012-1140
32. Prodromou, C., Roe, S., O'Brien, R., Ladbury, J., Piper, P., Pearl, L., *et al.* (1997) Identification and structural characterization of the ATP/ADP-binding site in the Hsp90 molecular chaperone. *Cell* **90**, 65–75
33. Stebbins, C. E., Russo, A., Schneider, C., Rosen, N., Hartl, F., Pavletich, N., *et al.* (1997) Crystal structure of an Hsp90-geldanamycin complex: targeting of a protein chaperone by an antitumor agent. *Cell* **89**, 239–250
34. Obermann, W. M. J., Sondermann, H., Russo, A. A., Pavletich, N. P., and Hartl, F. U. (1998) In Vivo function of Hsp90 is dependent on ATP binding and ATP hydrolysis. *J. Cell Biol.* **143**, 901–910
35. Panaretou, B., Prodromou, C., Roe, S., O'Brien, R., Ladbury, J., Piper, P., *et al.* (1998) ATP binding and hydrolysis are essential to the function of the Hsp90 molecular chaperone in vivo. *EMBO J.* **17**, 4829–4836
36. Patricia Hernández, M., Sullivan, W. P., and Toft, D. O. (2002) The assembly and intermolecular properties of the hsp70-Hop-hsp90 molecular chaperone complex. *J. Biol. Chem.* https://doi.org/10.1074/jbc.M206566200

37. Bagatell, R., Khan, O., Paine-Murrieta, G., Taylor, C., Akinaga, S., Whitesell, L., *et al.* (2001) Destabilization of steroid receptors by heat shock protein 90-binding drugs: a ligand-independent approach to hormonal therapy of breast cancer. *Clin. Cancer Res.*
38. Egorin, M. J., Rosen, D., Wolff, J., Callery, P., Musser, S., Eiseman, J., *et al.* (1998) Metabolism of 17-(allylamino)-17-demethoxygeldanamycin (NSC 330507) by murine and human hepatic preparations. *Cancer Res.*
39. McCollum, A. K., Teneyck, C. J., Sauer, B. M., Toft, D. O., and Erlichman, C. (2006) Up-regulation of heat shock protein 27 induces resistance to 17-allylamino-demethoxygeldanamycin through a glutathione-mediated mechanism. *Cancer Res.* https://doi.org/10.1158/0008-5472.CAN-06-1629
40. Clarke, P. A., Hostein, I., Banerji, U., Di Stefano, F., Maloney, A., Walton, M., *et al.* (2000) Gene expression profiling of human colon cancer cells following inhibition of signal transduction by 17-allylamino-17-demethoxygeldanamycin, an inhibitor of the hsp90 molecular chaperone. *Oncogene.* https://doi.org/10.1038/sj.onc.1203753
41. Erlichman, C. (2009) Tanespimycin: the opportunities and challenges of targeting heat shock protein 90. *Expert Opin. Investig. Drugs.* https://doi.org/10.1517/13543780902953699
42. Takayama, S., Reed, J. C., and Homma, S. (2003) Heat-shock proteins as regulators of apoptosis. Oncogene *Preprint at.* https://doi.org/10.1038/sj.onc.1207114
43. Zhao, Z., Wang, L., James, T., Jung, Y., Kim, I., Tan, R., *et al.* (2015) Reciprocal regulation of ERα and ERβ stability and activity by diptoindonesin G. *Chem. Biol.* https://doi.org/10.1016/j.chembiol.2015.10.011
44. Liu, J. T., Do, T., Simmons, C., Lynch, J., Gu, W., Ma, Z., *et al.* (2016) Total synthesis of diptoindonesin G and its analogues as selective modulators of estrogen receptors. *Org. Biomol. Chem.* https://doi.org/10.1039/c6ob01657j
45. Gao, J., Fan, M., Xiang, G., Wang, J., Zhang, X., Guo, W., *et al.* (2017) Diptoindonesin G promotes ERK-mediated nuclear translocation of p-STAT1 (Ser727) and cell differentiation in AML cells. *Cell Death Dis.* https://doi.org/10.1038/cddis.2017.159
46. Fan, M., Chen, J., Gao, J., Xue, W., Wang, Y., Li, W., *et al.* (2020) Triggering a switch from basal- to luminal-like breast cancer subtype by the small-molecule diptoindonesin G via induction of GABARAPL1. *Cell Death Dis.* https://doi.org/10.1038/s41419-020-02878-z
47. Mao, F., Kong, Y., Liu, J., Rao, X., Li, C., Donahue, K., *et al.* (2022) Diptoindonesin G antagonizes AR signaling and enhances the efficacy of anti-androgen therapy in prostate cancer. *Prostate*
48. Brünner, N., Frandsen, T., Holst-Hansen, C., Bei, M., Thompson, E., Wakeling, A., *et al.* (1993) MCF7/LCC2: a 4-hydroxytamoxifen resistant human breast cancer variant that retains sensitivity to the steroidal antiestrogen ICI 182,780. *Cancer Res.*
49. Ran, F. A., Hsu, P., Wright, J., Agarwala, V., Scott, D., Zhang, F., *et al.* (2013) Genome engineering using the CRISPR-Cas9 system. *Nat. Protoc.* https://doi.org/10.1038/nprot.2013.143
50. Donnelly, A., and Blagg, B. (2008) Novobiocin and additional inhibitors of the Hsp90 C-terminal nucleotide- binding pocket. *Curr. Med. Chem.* https://doi.org/10.2174/092986708786242895
51. Soti, C., Vermes, Á., Haystead, T. A. J., and Csermely, P. (2003) Comparative analysis of the ATP-binding sites of Hsp90 by nucleotide affinity cleavage: a distinct nucleotide specificity of the C-terminal ATP-binding site. *Eur. J. Biochem.* **270**
52. Roe, S. M., Prodromou, C., O'Brien, R., Ladbury, J., Piper, P., Pearl, L., *et al.* (1999) Structural basis for inhibition of the Hsp90 molecular chaperone by the antitumor antibiotics radicicol and geldanamycin. *J. Med. Chem.* https://doi.org/10.1021/jm980403y
53. Fontana, J., Fulton, D., Chen, Y., Fairchild, T., McCabe, T., Fujita, N., *et al.* (2002) Domain mapping studies reveal that the M domain of hsp90 serves as a molecular scaffold to regulate Akt-dependent phosphorylation of endothelial nitric oxide synthase and NO release. *Circ. Res.* https://doi.org/10.1161/01.RES.0000016837.26733
54. Robinson, M. B., Tidwell, J., Gould, T., Taylor, A., Newbern, J., Graves, J., *et al.* (2005) Extracellular heat shock protein 70: a critical component for motoneuron survival. *J. Neurosci.* **25**
55. Burlison, J. A., Avila, C., Vielhauer, G., Lubbers, D., Holzbeierlein, J., Blagg, B., *et al.* (2008) Development of novobiocin analogues that manifest anti-proliferative activity against several cancer cell lines. *J. Org. Chem.* https://doi.org/10.1021/jo702191a
56. Corsello, S. M., Nagari, R., Spangler, R., Rossen, J., Kocak, M., Bryan, J., *et al.* (2020) Discovering the anticancer potential of non-oncology drugs by systematic viability profiling. *Nat. Cancer.* https://doi.org/10.1038/s43018-019-0018-6
57. Yu, C., Mannan, A., Yvone, G., Ross, K., Zhang, Y., Marton, M., *et al.* (2016) High-throughput identification of genotype-specific cancer vulnerabilities in mixtures of barcoded tumor cell lines. *Nat. Biotechnol.* https://doi.org/10.1038/nbt.3460
58. Bahreini, A., Li, Z., Wang, P., Levine, K., Tasdemir, N., Cao, L., *et al.* (2017) Mutation site and context dependent effects of ESR1 mutation in genome-edited breast cancer cell models. *Breast Cancer Res.* https://doi.org/10.1186/s13058-017-0851-4
59. Guillen, K. P., Fujita, M., Butterfield, A., Scherer, S., Bailey, M., Chu, Z., *et al.* (2022) A human breast cancer-derived xenograft and organoid platform for drug discovery and precision oncology. *Nat. Cancer* **3**
60. Morishima, Y., Wang, A., Yu, Z., Pratt, W., Osawa, Y., Lieberman, A., *et al.* (2008) CHIP deletion reveals functional redundancy of E3 ligases in promoting degradation of both signaling proteins and expanded glutamine proteins. *Hum. Mol. Genet.* https://doi.org/10.1093/hmg/ddn296
61. Zhang, Y., Dayalan Naidu, S., Samarasinghe, K., Van Hecke, G., Pheely, A., Boronina, T., *et al.* (2014) Sulphoxythiocarbamates modify cysteine residues in HSP90 causing degradation of client proteins and inhibition of cancer cell proliferation. *Br. J. Cancer* **110**
62. Hu, Y., and Mivechi, N. F. (2003) HSF-1 interacts with Ral-binding protein 1 in a stress-responsive, multiprotein complex with HSP90 *in vivo*. *J. Biol. Chem.* **278**
63. Jolly, C., and Morimoto, R. I. (2000) Role of the heat shock response and molecular chaperones in oncogenesis and cell death. *J. Natl. Cancer Inst.* **92.** https://doi.org/10.1093/jnci/92.19.1564
64. Tateishi, Y., Kawabe, Y., Chiba, T., Murata, S., Ichikawa, K., Murayama, A., *et al.* (2004) Ligand-dependent switching of ubiquitin-proteasome pathways for estrogen receptor. *EMBO J.* https://doi.org/10.1038/sj.emboj.7600472
65. Long, X., and Nephew, K. P. (2006) Fulvestrant (ICI 182,780)-dependent interacting proteins mediate immobilization and degradation of estrogen receptor-α. *J. Biol. Chem.* https://doi.org/10.1074/jbc.M510809200
66. Li, D., Kawabe, Y., Chiba, T., Murata, S., Ichikawa, K., Murayama, A., *et al.* (2016) Natural product kongensin A is a non-canonical HSP90 inhibitor that blocks RIP3-dependent necroptosis. *Cell Chem. Biol.* https://doi.org/10.1016/j.chembiol.2015.08.018
67. Zhang, F. Z., Ho, D. H. H., and Wong, R. H. F. (2018) Triptolide, a HSP90 middle domain inhibitor, induces apoptosis in triple manner. *Oncotarget* **9**
68. Yim, K. H., Prince, T., Qu, S., Bai, F., Jennings, P., Onuchic, J., *et al.* (2016) Gambogic acid identifies an isoform-specific druggable pocket in the middle domain of Hsp90β. *Proc. Natl. Acad. Sci. U S A.* **113**
69. Yu, Y., Hamza, A., Zhang, T., Gu, M., Zou, P., Newman, B., *et al.* (2010) Withaferin A targets heat shock protein 90 in pancreatic cancer cells. *Biochem. Pharmacol.* https://doi.org/10.1016/j.bcp.2009.09.017
70. Li, N., Xu, M., Wang, B., Shi, Z., Zhao, Z., Tang, Y., *et al.* (2019) Discovery of novel celastrol derivatives as Hsp90-Cdc37 interaction disruptors with antitumor activity. *J. Med. Chem.* https://doi.org/10.1021/acs.jmedchem.9b01290
71. Hadden, M. K., Galam, L., Gestwicki, J. E., Matts, R. L., and Blagg, B. S. J. (2007) Derrubone, an inhibitor of the Hsp90 protein folding machinery. *J. Nat. Prod.* https://doi.org/10.1021/np070190s
72. Meyer, P., Prodromou, C., Liao, C., Hu, B., Roe, S., Vaughan, C., *et al.* (2004) Structural basis for recruitment of the ATPase activator Aha1 to the Hsp90 chaperone machinery. *EMBO J.* **23**
73. Yu, M., Bardia, A., Aceto, N., Bersani, F., Madden, M., Donaldson, M., *et al.* (2014) Ex vivo culture of circulating breast tumor cells for individualized testing of drug susceptibility. *Science (1979).* https://doi.org/10.1126/science.1253533

74. Dobin, A., Davis, C., Schlesinger, F., Drenkow, J., Zaleski, C., Jha, S., *et al.* (2013) STAR: ultrafast universal RNA-seq aligner. *Bioinformatics* **29**
75. Anders, S., Pyl, P. T., and Huber, W. (2015) HTSeq-A Python framework to work with high-throughput sequencing data. *Bioinformatics* **31**
76. Love, M. I., Huber, W., and Anders, S. (2014) Moderated estimation of fold change and dispersion for RNA-seq data with DESeq2. *Genome Biol.* **15**
77. Mootha, V. K., Daly, M., Patterson, N., Hirschhorn, J., Groop, L., Altshuler, D., *et al.* (2004) Reply to 'Statistical concerns about the GSEA procedure'. *Nat. Genet.* **36**, 663, 663
78. Subramanian, A., Tamayo, P., Mootha, V., Mukherjee, S., Ebert, B., Gillette, M., *et al.* (2005) Gene set enrichment analysis: a knowledge-based approach for interpreting genome-wide expression profiles. *Proc. Natl. Acad. Sci. U S A.* **102**

Kristine Donahue recently completed her doctoral studies in Cancer Biology at the University of Wisconsin–Madison in McArdle Laboratory under the guidance of Prof. Wei Xu. Studying diptoindonesin G's mechanism of action inspired a keen interest in modulating protein stability and the ubiquitin-proteasome system, which continues to drive her postdoctoral work at the Novartis Institutes for Biomedical Research.

Haibo Xie is a scientist in the School of Pharmacy at University of Wisconsin–Madison. He studies molecular mechanisms of diptoindonesin G (Dip G), identified Dip G as an HSP90 modulator that can promote degradation of HSP90 clients ERα by binding to the middle domain of HSP90.